

University of Bremen



Postgraduate Program Environmental Physics  
Institute for Environmental Physics

# **Transport of NO<sub>2</sub> by cyclones: Comparing model simulations and satellite observations**

Mason Ross Keith  
no. 295248-1

- |                    |                                     |
|--------------------|-------------------------------------|
| <i>1. Examiner</i> | Prof. Dr. John P. Burrows           |
| <i>2. Examiner</i> | PD Dr. Annette Ladstätter-Weißmayer |
| <i>Supervisor</i>  | Dr. Anne-Marlene Blechschmidt       |

July 23, 2015



Diese Erklärungen sind in jedes Exemplar der Bachelor- bzw. Masterarbeit mit einzubinden.

Name: \_\_\_\_\_ Matr.Nr.: \_\_\_\_\_

### **Urheberrechtliche Erklärung**

Hiermit versichere ich, dass ich die vorliegende Arbeit selbstständig verfasst und keine als die angegebenen Quellen und Hilfsmittel verwendet habe.

Alle Stellen, die ich wörtlich oder sinngemäß aus anderen Werken entnommen habe, habe ich unter Angabe der Quellen als solche kenntlich gemacht.

---

Datum

Unterschrift

### **Erklärung zur Veröffentlichung von Abschlussarbeiten**

Die Abschlussarbeit wird zwei Jahre nach Studienabschluss dem Archiv der Universität Bremen zur dauerhaften Archivierung angeboten.

Archiviert werden:

- 1) Masterarbeiten mit lokalem oder regionalem Bezug sowie pro Studienfach und Studienjahr 10 % aller Abschlussarbeiten
- 2) Bachelorarbeiten des jeweils ersten und letzten Bachelorabschlusses pro Studienfach und Jahr.

- Ich bin damit einverstanden, dass meine Abschlussarbeit im Universitätsarchiv für wissenschaftliche Zwecke von Dritten eingesehen werden darf
- Ich bin damit einverstanden, dass meine Abschlussarbeit nach 30 Jahren (gem. §7 Abs. 2 BremArchivG) im Universitätsarchiv für wissenschaftliche Zwecke von Dritten eingesehen werden darf.
- Ich bin nicht damit einverstanden, dass meine Abschlussarbeit im Universitätsarchiv für wissenschaftliche Zwecke von Dritten eingesehen werden darf

---

Datum

Unterschrift



# Abstract

The effects of tropospheric nitrogen dioxide ( $\text{NO}_2$ ) are felt by humans and the environment in several ways. In the troposphere, ozone formation by  $\text{NO}_2$  is hazardous to humans. The formation of acid rain from the chemical reaction between  $\text{NO}_2$  and OH is also harmful to the environment. Long range transport (LRT) events caused by vertical lifting of  $\text{NO}_2$  within cyclones into the upper troposphere significantly increase the lifetime of  $\text{NO}_2$  and can then influence not only regional but also global air quality. Correct representation of  $\text{NO}_2$  LRT events is a challenge for numerical models due to  $\text{NO}_2$ 's short lifetime and high chemical reactivity.

In this study, a case study of an LRT event is presented in which a large plume of  $\text{NO}_2$  was transported in an extra tropical cyclone from the emission region over the UK and Northern Europe towards Iceland and the North Atlantic ocean. Results of MACC-II Reanalysis and WRF-Chem models will be compared to GOME-2 satellite observations of tropospheric  $\text{NO}_2$  columns. This is done in order to verify the performance of these widely used global and regional chemistry models. The whole lifetime of the  $\text{NO}_2$  plume will be investigated including sources and conversion into different species.

Results show that both models are able to represent long range transport of  $\text{NO}_2$  in the cyclone. The concentration of  $\text{NO}_2$  in the plume is lower in the models than that of the satellite retrieval due in part to chemical conversion of  $\text{NO}_2$ . We also show that increased model resolution leads to better agreement between model and satellite data.



# Acknowledgement

Firstly, I would like to express my sincere gratitude to my adviser Dr. Anne-Marlene Blechschmidt for the continuous support of my MSc. study and related research, for her patience, motivation, and immense knowledge. Her guidance helped me in all the time of research and writing of this thesis. I could not have imagined having a better adviser and mentor for my MSc. study.

In addition to my adviser, I would like to thank my examiners: Prof. Dr. John P. Burrows, and PD Dr. Annette Ladstätter-Weißenmayer, for their insightful comments and encouragement, but also for the hard question which incensed me to widen my research from various perspectives.

My sincere thanks also goes IUP who provided me an opportunity to join their team while completing my study. Without their support it would not be possible to conduct this study.

Last but not the least, I would like to thank my family for supporting me spiritually throughout writing this thesis and my my life in general.



# Contents

<b>1</b>	<b>Introduction</b>	<b>1</b>
<b>2</b>	<b>Background</b>	<b>7</b>
2.1	Cyclones: Vertical transport processes . . . . .	7
2.2	Sources and sinks of NO <sub>2</sub> . . . . .	10
2.3	Chemistry of NO <sub>2</sub> in the troposphere . . . . .	12
2.4	Effects of NO <sub>2</sub> on human health . . . . .	14
2.5	Satellite based retrievals of NO <sub>2</sub> : DOAS . . . . .	15
<b>3</b>	<b>Outline and description</b>	<b>21</b>
3.1	GOME-II satellite retrievals . . . . .	21
3.2	Chemistry transport models . . . . .	22
3.2.1	MACC-II . . . . .	23
3.2.2	WRF-Chem . . . . .	24
3.3	Method of approach . . . . .	25
<b>4</b>	<b>Results</b>	<b>27</b>
4.1	NO <sub>2</sub> Long Range Transport . . . . .	27
4.2	GOME-2 vs. MACC-II Reanalysis . . . . .	29
4.3	MACC-II Reanalysis vs. WRF-Chem 100km . . . . .	31
4.4	GOME-2 vs. WRF-Chem 50km . . . . .	34
4.5	WRF-Chem chemistry diagnostics . . . . .	36
4.5.1	NO <sub>2</sub> Chemical Conversion . . . . .	37
4.5.2	HNO <sub>3</sub> Wet Scavenging . . . . .	41
4.5.3	HNO <sub>3</sub> Transport . . . . .	43
4.5.4	PAN Transport . . . . .	45
<b>5</b>	<b>Summary</b>	<b>47</b>
<b>6</b>	<b>Outlook</b>	<b>51</b>
	<b>Bibliography</b>	<b>53</b>

<b>A Appendices</b>	<b>57</b>
A.1 GOME-2 . . . . .	57
A.2 MACC-II Reanalysis . . . . .	59
A.3 WRF-Chem . . . . .	68
A.3.1 100km resolution NO <sub>2</sub> . . . . .	69
A.3.2 50km resolution NO <sub>2</sub> . . . . .	75

# Introduction

The short lifetime of  $\text{NO}_2$  in the planetary boundary layer (PBL) typically makes the chances of long range transport (LRT) very low. The PBL is the lowest part of the atmosphere and its behavior is directly influenced by its contact with the planets surface. Most LRT events are associated with long-lived chemical species such as  $\text{CO}$ ,  $\text{SO}_2$ , and  $\text{O}_3$  where these trace gases are transported over long distances from their original emission source. However, certain weather conditions, such as transport by cyclones, make it possible for short lived species such as  $\text{NO}_2$  to be transported over long distances.

When  $\text{NO}_2$  is transported into the upper troposphere, the lifetime of the trace gas increases from several hours to several days depending on the strength of solar irradiation and available radicals (Ehhalt *et al.* [16]). Using satellite remote sensors, it is possible to observe these LRT events and then compare the data to numerical models in order to better understand performance of simulations for the transport of short lived species in our atmosphere.

$\text{NO}_2$  is toxic to humans. It reacts with several species in the atmosphere such as  $\text{OH}$  and  $\text{O}_3$ . It is also photolysed by sunlight and can form acid rain, ozone, and other compounds. The small particles formed as a result of  $\text{NO}_x$  reacting with ammonia, moisture, and other compounds penetrate the lungs and can cause respiratory disease such as bronchitis and emphysema. These particles can also aggravate or worsen certain heart diseases leading to premature death (<http://www.epa.gov>). Photochemical smog is the product of the photolization process of  $\text{NO}_2$  amplified by the presence of  $\text{OH}$  and volatile organic compounds. Since the lifetime of  $\text{NO}_2$  is typically short, photochemical smog is usually limited to the emission region. Results by Zien *et al.* [36] have shown that a LRT event over the polluted region can transport

the NO<sub>2</sub> to pristine regions otherwise not polluted by typical emission sources.

Current representation of the transport of NO<sub>2</sub> is a challenge for numerical models due to complex chemical interactions of NO<sub>2</sub> with other species in varying parts of the atmosphere. Moreover, simulating the lifting of NO<sub>2</sub> out of the PBL into the free troposphere is critical, as the short lifetime of NO<sub>2</sub> is significantly enhanced in the free troposphere. The models must transport the NO<sub>2</sub> out of the boundary layer quickly enough to not be converted into other species. Sources and sinks of NO<sub>2</sub> must be accounted for and represented in order to understand the complete process of LRT. This case study is based on an event from the data set of LRT events by Zien *et al.* [36] in which an extra tropical cyclone passed over the UK and northern Europe, and will investigate sources and sinks of NO<sub>2</sub> using data from the global MACC-II Reanalysis and the regional WRF-Chem models. The model data will be compared to satellite data received from the GOME-II instrument aboard the METOP-A satellite in order to better understand their performance.

A long range transport event is defined as a distinct plume of trace gases being exported from an emission region to a downwind region over a long distance (OECD [29]). Due to the short lifetime of NO<sub>2</sub> in the lower troposphere, LRT will predominantly happen in the free troposphere. According to Ehhalt *et al.* [16], the lifetime for NO<sub>2</sub> in the PBL lasts between 8 hours over continents due to dry deposition from the reaction of NO<sub>2</sub> and OH and 10 hours over oceans due to reactions with OH and water vapor. The lifetime of NO<sub>2</sub> in the free troposphere is approximately 9 days depending on irradiance and available chemical species. Since LRT is a large scale event, we use satellite retrievals of tropospheric NO<sub>2</sub> for analysis. According to Zien *et al.* [36], LRT events of NO<sub>2</sub> are rarely seen and often overlooked in satellite retrievals. This is due to cloud corrections performed on the satellite data that will eliminate the LRT from the data, whereas in most cases, the LRT of NO<sub>2</sub> can be attributed to weather systems suddenly lifting the trace gas

into the free troposphere. A cloud filter is usually applied to the satellite data because of problems associated with the difficulty of estimating the amount of gases of interest beneath the clouds due to the shielding effect (Beirle *et al.* [5]). Moreover, the sensitivity of the retrieval may be enhanced if the  $\text{NO}_2$  is located within or above a cloud (Zien *et al.* [36]). The LRT events observed for  $\text{NO}_2$  are usually accompanied by clouds in the location of fronts which indicate vertical lifting. Zien *et al.* [36] omitted the cloud filter and as such was able to detect 3808 verified  $\text{NO}_2$  LRT events in the GOME-2 data between 2007 and 2011.

Several studies have investigated individual  $\text{NO}_2$  LRT events based on satellite and model data. Stohl *et al.* [33] investigated an episode in November of 2001 where an intense low pressure system transported  $\text{NO}_2$  pollution across the Atlantic in as little as a day due to strong vertical uplift and high wind speeds.

Wenig *et al.* [35] described one of the first satellite observations of  $\text{NO}_x$  transport over long distances. The satellite observed emissions from power plants, and the satellite data was verified by a particle tracer model. They showed that  $\text{NO}_x$  could be transported thousands of kilometers from its emission source.

Beirle *et al.* [5] presented a method for the determination of the emissions of city  $\text{NO}_x$  as well as lifetimes of  $\text{NO}_x$  from satellite measurements by analyzing downwind patterns of  $\text{NO}_2$  for different wind conditions. They found that  $\text{NO}_x$  emissions retrieved by the satellite sensors generally agree with emission inventories of the cities used by numerical models.

Schaub *et al.* [32] described an event in southern Germany where  $\text{NO}_2$  was vertically transported into the free troposphere and then transported towards the Alps. GOME retrievals of  $\text{NO}_2$  were verified by in situ measurements conducted in the Alps by ozone chemiluminescence detectors.

Ding *et al.* [15] conducted an aircraft campaign in north east China in order to study the role of cyclones for the transport of air pollutants. They found that emissions from mega-cities in China were lifted into the free troposphere by a front crossing over a mountain range. The pollution was further lifted into the upper troposphere by a warm conveyor belt and exported from Asia to North America.

Lin *et al.* [27] used the Weather Research and Forecasting (WRF) and Community Multi-scale Air Quality Model (CMAQ) to model pollution transport over the Asian continent with high resolution. They found that both models were not able to adequately represent the rapid venting through deep convection on the leading edge of frontal systems when compared to aircraft observations.

Barth *et al.* [4] compared how several different species are transported in small scale convective systems like thunderstorms. Using high resolution cloud chemistry models, they were able to show that transport of different gas species compares well between models, but mixing ratios of soluble species showed significant differences due to the role of the ice phase, the impact of cloud-modified photolysis rates on the chemistry, and the representation of the species chemical reactivity.

Klich and Fuelberg [25] used the WRF-Chem model to simulate a cyclone in East Asia in order to study the transport of CO. The model was run at three different resolutions and showed that convection due to vertical transport accounted for a large portion of the transport of CO.

In this study, we investigate a LRT event in which NO<sub>2</sub> was transported from the UK and central Europe in October of 2010. This event was taken from the database of LRT events detected by Zien *et al.* [36]. This event shows clear LRT of NO<sub>2</sub> in the GOME-II data without cloud correction. This event can also be linked to a cyclone appearing over the area at the same time. We compare the satellite retrievals from Zien *et al.* [36] with two different models, one

global chemistry transport model and a regional high resolution model, in order to verify performance of the models compared to the satellite and to see if increased resolution in model simulations lead to better agreement with the satellite data. We will show that both models are able to represent LRT transport to a certain extent but chemistry and physics settings in the models seem to play a large role in how well the models perform. We will also show that with increased resolution comes better agreement between satellite and model data.

In the following chapters, a background of transport in cyclones and chemistry of the troposphere will be given, followed by an explanation of DOAS retrievals. The data sets used will be detailed and then the results will be presented followed by a summary and outlook.



## Background

### 2.1 Cyclones: Vertical transport processes

A cyclone is a system of winds rotating inwards towards an area of low pressure with an anticlockwise rotation in the northern hemisphere. The process of the development of the cyclone is called cyclogenesis. At mid-latitudes, this involves the interaction of warmer sub tropical air and colder polar air at the polar front. The interaction of the two air masses causes the warm air to be lifted. The Norwegian cyclone model, developed by V. and J. Bjerknes, described the formation of an idealized cyclone. Figure 2.1 shows a schematic of idealized cyclone development. As the cyclone moves Eastwards, it is seen that the warm front is being followed by a cold front with a section of warm air between. As the cold front catches the warm front, an occlusion occurs. Vertical lifting occurs at all parts of the front including the cold front, warm front, and the occlusion. The occlusion is the region with the greatest intensity of the cyclone.

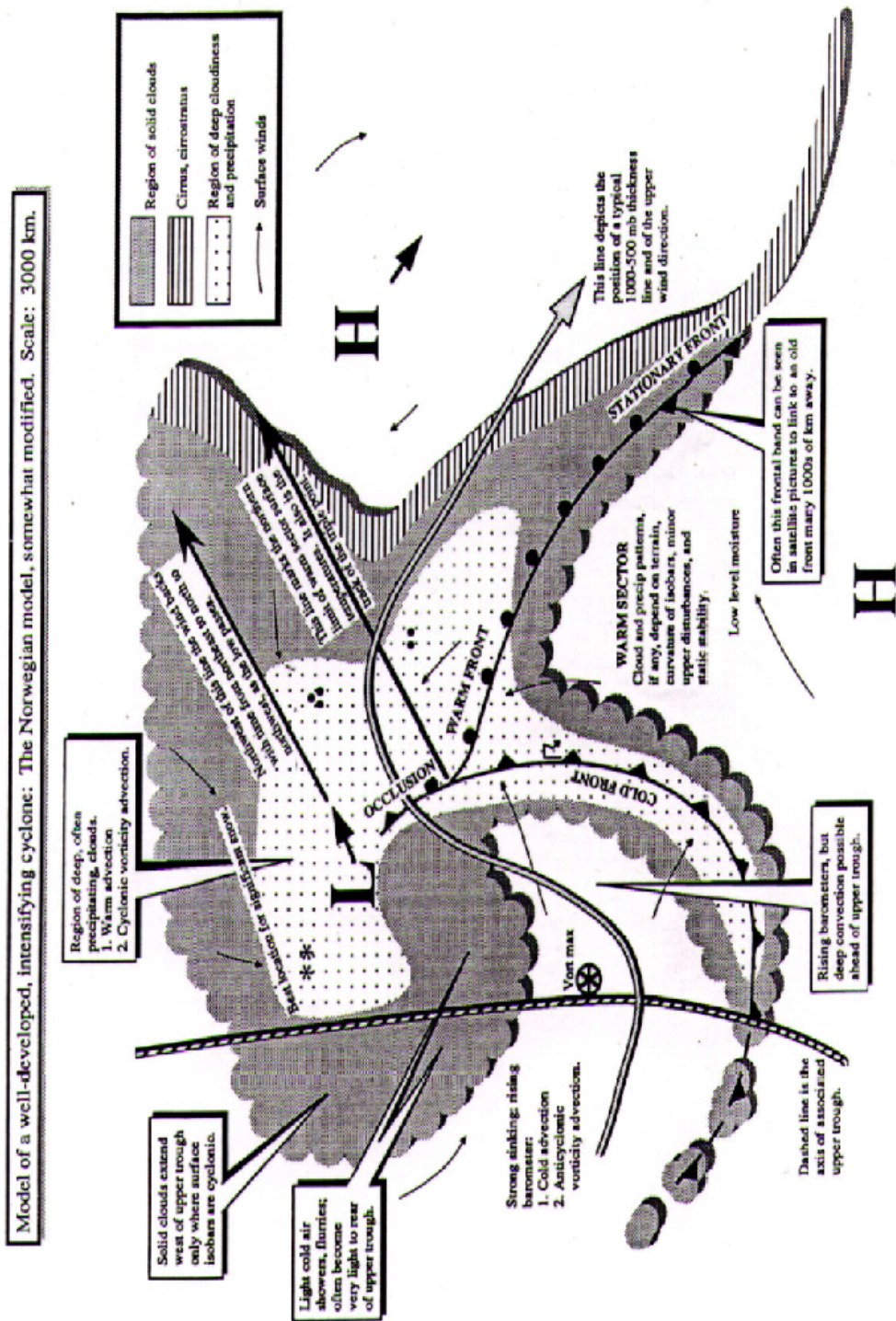
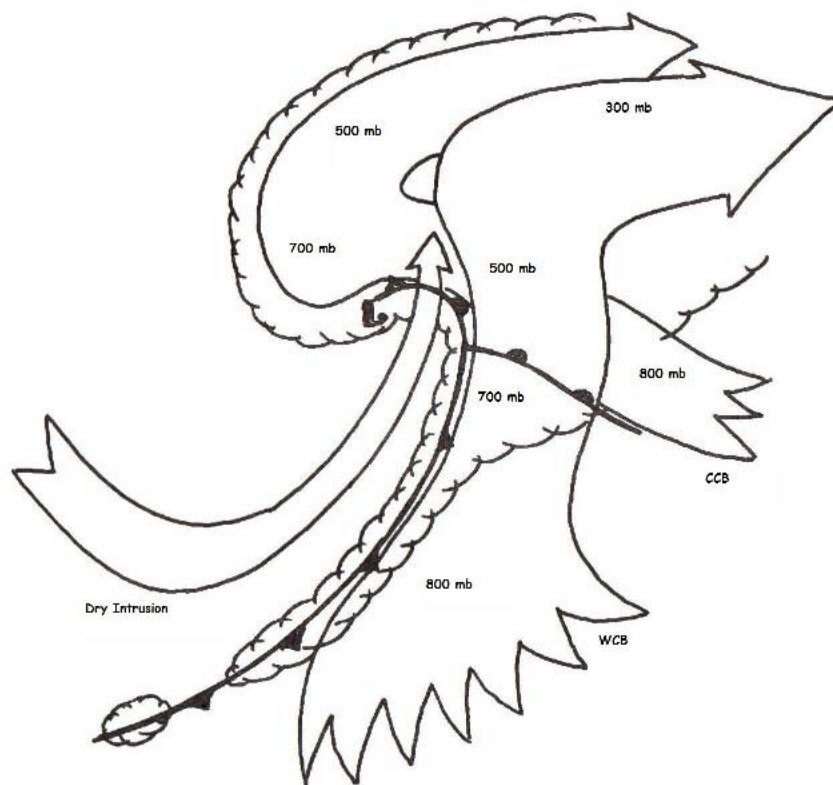


Fig. 2.1.: Idealized Cyclone represented by the Norwegian cyclone model. (Horstmeyer [20])

A so called "warm conveyor belt" (figure 2.2) is the stream of warm moist air that ascends the cooler air of the cold front (Horstmeyer [20]). The warm



**Fig. 2.2.:** Drawing showing the three main conveyor belts associated with a northern hemisphere extra tropical cyclone. the warm conveyor belt (wcb), the cold conveyor belt (ccb), and dry intrusion. (<http://www.wxonline.info/topics/convey2a.jpg>)

conveyor belt transports warm moist air northward overtaking the cold air as it ascends.

As the warm air mass reaches higher altitude, it then turns eastward. The cold conveyor belt is a flow of air characterized by lower temperatures that flows rearwards, relative to the advancing system (2.2). Also depicted is cloud free dry intrusion. This dry intrusion is caused by dry air descending from the lower stratosphere through a troposphere fold into the center of the cyclone (<http://www.met.reading.ac.uk/storms/>). Ascent along the cold front can be very intense and is potentially what leads to LRT events of short lived trace gases. The combination of the warm and cold conveyor belts in cyclones is what drives LRT of trace gasses.

## 2.2 Sources and sinks of NO<sub>2</sub>

The earth's atmosphere is made up of a mixture of gases and suspended particles. It consists of several layers and partly absorbs the incoming radiation from the sun. The lowest level of the atmosphere is the troposphere which ranges from 0-15 km. The troposphere is heated from the bottom up due to reflected solar radiation from the surface and the temperature gradually decreases with increasing altitude until the top of the troposphere or tropopause. The atmosphere is made up primarily of Nitrogen (78.084 %), Oxygen (20.946 %), Argon (0.9340 %), and Carbon dioxide (0.0397 %) with small amounts of other trace gases mixed in it. NO<sub>x</sub> is the term referring to the sum of Nitrogen Oxides NO and NO<sub>2</sub> (NO<sub>x</sub>=NO+NO<sub>2</sub>). NO<sub>x</sub> is primarily emitted as NO in the atmosphere, but is quickly converted to NO<sub>2</sub> during the day through the null cycle.



The formation of NO<sub>2</sub> is both natural and anthropogenic. Humans contribute to the formation of NO<sub>2</sub> through combustion processes such as the burning of fuel on coal, oil, and power plants which accounts for approximately half of total NO<sub>2</sub> emissions Jacob [24]. Biomass burning is another significant source of NO<sub>2</sub> emissions. This is mostly due to tropical agriculture in which forests or crops are burned to clear land for new crops. The extreme temperatures associated with lightning strikes also produces NO<sub>2</sub>. Table 2.1 shows the estimated sources of tropospheric emissions of NO<sub>x</sub> (Jacob [24]).

The primary sink of NO<sub>2</sub> is oxidation to HNO<sub>3</sub>. In the troposphere, HNO<sub>3</sub> is removed from the atmosphere through wet scavenging, producing acid rain. This hinders the LRT of NO<sub>2</sub> in the troposphere. An important reservoir

	Source, Tg N yr <sup>-1</sup>
Fossil fuel combustion	21
Biomass burning	12
Soils	6
Lightning	3
NH <sub>3</sub> oxidation	3
Aircraft	0.5
Transport from stratosphere	0.1

**Tab. 2.1.:** Table showing estimated sources of NO<sub>x</sub> in the troposphere, taken from (Jacob [24]).

for NO<sub>2</sub> is Peroxyacetylnitrate (PAN). PAN is not highly soluble by water and is therefore not subject to deposition like HNO<sub>3</sub> is. The lifetime of PAN is dependent on temperature. At 250K, the life span of PAN can be several months (Jacob [24]). This allows PAN to be transported over long distances in the free troposphere and subsequent conversion to NO<sub>2</sub> can occur if the plume subsides to lower, warmer altitudes. The lifetime of NO<sub>x</sub> is only several hours at the surface, but increases with increasing height. Figure 2.3 shows the lifetime of NO<sub>x</sub> versus the height.

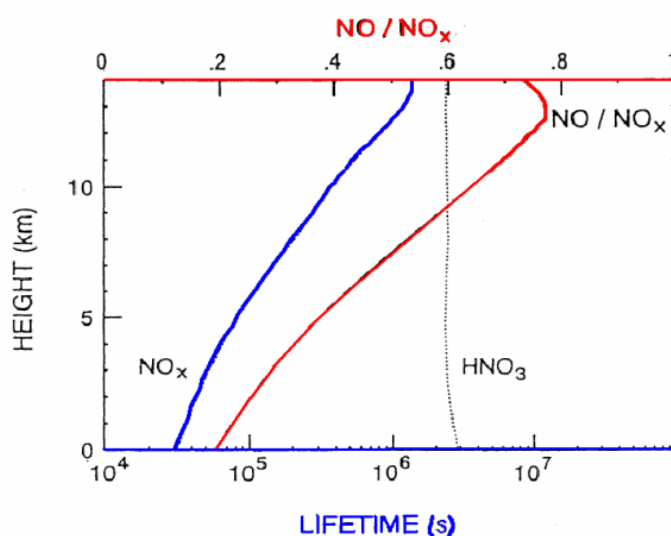


**Fig. 2.3.:** Atmospheric lifetime of NO<sub>x</sub> in the troposphere (Ehhalt *et al.* [16])

## 2.3 Chemistry of NO<sub>2</sub> in the troposphere

NO<sub>2</sub> plays a large role in the chemical equilibrium of the troposphere. In the PBL, the combustion of fossil fuels creates NO through the reaction:

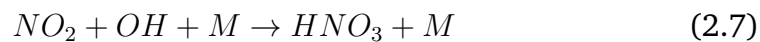


NO<sub>2</sub> is then created through the reaction:

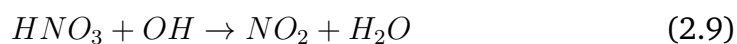


This reaction is very fast.

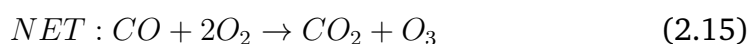
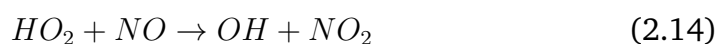
During the day, NO<sub>2</sub> is converted into HNO<sub>3</sub> through the reaction with the hydroxyl radical OH. In a cyclone, rain is expected to accompany the fronts. This leads to wet scavenging.



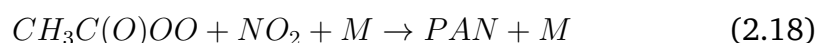
The HNO<sub>3</sub> acts as a sink for the NO<sub>2</sub> since HNO<sub>3</sub> is highly susceptible to wet deposition. The reverse reaction



allows  $\text{HNO}_3$  to be converted back into  $\text{NO}_2$  but the reaction is very slow and is therefore less important (Ehhalt *et al.* [16]). In the troposphere,  $\text{NO}_2$  is also involved in the production of  $\text{O}_3$  through the reaction



The creation of  $\text{O}_3$  is detrimental to human health by leading to respiratory problems. PAN is produced through the equation:



PAN as a reservoir of  $\text{NO}_2$  is not affected by wet scavenging and can be transported from polluted regions to pristine regions causing problems in remote areas. As the PAN warms, it regenerates  $\text{NO}_2$  through thermal decomposition

Jacob [24]. A cyclone can transport PAN to the free troposphere where it can travel long distances. If the plume warms again through subsidence, it can reproduce  $\text{NO}_2$  through the reaction:



During the nighttime, there is no sunlight, and there is then very little OH for the  $\text{NO}_2$  to react with. Instead,  $\text{NO}_2$  reacts with  $\text{NO}_3$ .  $\text{NO}_3$  is formed from the reaction between  $\text{NO}_2$  and  $\text{O}_3$ . The  $\text{NO}_2$  and  $\text{NO}_3$  react with each other to form a chemical equilibrium with  $\text{N}_2\text{O}_5$ .



In order for  $\text{NO}_2$  to be transported in the cyclone, the vertical transport has to be fast enough for the  $\text{NO}_2$  to not be converted into  $\text{HNO}_3$  or PAN as there are generally higher concentrations of radicals in the boundary layer than in the free troposphere.

## 2.4 Effects of $\text{NO}_2$ on human health

In the troposphere, increased concentrations of  $\text{NO}_2$  can have long lasting health effects. These effects range from light headache and cough, to capillary damage and inflation of the respiratory tract. People with asthma are especially susceptible to the effects of  $\text{NO}_2$ . If long enough concentrated exposure to  $\text{NO}_2$  occurs, bronchitis and respiratory failure may occur. The Air Quality Index gives recommended exposure levels to  $\text{NO}_2$  shown in Figure 2.4.

## Air Quality Guide for Nitrogen Dioxide

Air Quality Index	Protect Your Health Near Roadways
Good (0-50)	No health impacts are expected when air quality is in this range.
Moderate (51-100)	Individuals who are unusually sensitive to nitrogen dioxide should <u>consider limiting prolonged</u> outdoor exertion.
Unhealthy for Sensitive Groups (101-150)	The following groups should <u>limit prolonged</u> outdoor exertion: <ul style="list-style-type: none"> <li>• People with lung disease, such as asthma</li> <li>• Children and older adults</li> </ul>
Unhealthy (151-200)	The following groups should <u>avoid prolonged</u> outdoor exertion: <ul style="list-style-type: none"> <li>• People with lung disease, such as asthma</li> <li>• Children and older adults</li> </ul> Everyone else should <u>limit prolonged</u> outdoor exertion.
Very Unhealthy (201-300)	The following groups should <u>avoid all</u> outdoor exertion: <ul style="list-style-type: none"> <li>• People with lung disease, such as asthma</li> <li>• Children and older adults</li> </ul> Everyone else should <u>limit</u> outdoor exertion.

Fig. 2.4.: <http://www.epa.gov/airnow/no2.pdf>

The air quality index is produced by the EPA in accordance with the Clean Air Act. A comprehensive risk assessment is done drawing on the most up to date information associated with risks to human health.

## 2.5 Satellite based retrievals of NO<sub>2</sub>: DOAS

DOAS (Differential Optical Absorption Spectroscopy) is a well established technique for deriving the amount of trace gases in the atmosphere. These concentrations are derived from measurements of light in the UV/visible and near infrared spectral range. Different species are separated in the satellite data by looking at the measurements in limited spectral bands. DOAS relies on the following principle: as solar radiation passes through the atmosphere, different molecules absorb the radiation at different wavelengths. By observing the absorption spectra, we are able to derive the information about the concentrations of molecules in the atmosphere.

The DOAS method only analyzes signals that vary rapidly with wavelength. This is expressed as the 'Differential' in DOAS. The DOAS method is applied to many different measuring platforms and can target several gas species at the same time. Target species that can be retrieved from DOAS are H<sub>2</sub>O, HONO, HCHO, CHOCHO, O<sub>3</sub>, NO<sub>2</sub>, NO<sub>3</sub>, and BrO. Figure 2.5 shows different absorption cross sections of atmospheric species.

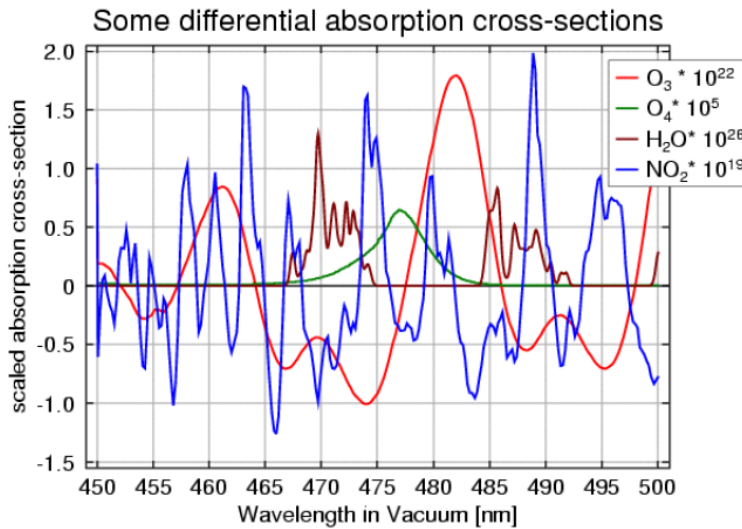


**Fig. 2.5.:** DOAS cross sections of different species Source: Measurement Techniques in Environmental Physics (2006) Richter

DOAS relies on the Beer-Lambert law. For a homogeneous medium, it is represented by:

$$I(\lambda) = I_0(\lambda)e^{-\sigma(\lambda)\rho l} \quad (2.22)$$

where  $I_0(\lambda)$  is un-attenuated spectral intensity,  $I(\lambda)$  is the measured spectral intensity,  $\rho$  = density of absorber,  $\lambda$  = wavelength,  $\sigma$  = absorption cross-section of absorber, and  $l$  is the path length also called the slant column.  $\rho l$  is the total amount of absorber along the light path. Since the atmosphere is not homogeneously distributed along the light path, the observed absorption

is then considered the absorption along the individual light paths weighted by respective intensity. The Lambert Beer law is modified to be:

$$I(\lambda) = I_0(\lambda)e^{-\int \sum \sigma(\lambda)\rho dl} \quad (2.23)$$

The Lambert Beer law is then used for finding the slant column, accounting for the extinction by molecular absorption of different species, Mie and Rayleigh scattering. The cross sections of both types of scattering are introduced into the equation giving:

$$I(\lambda) = a(\lambda, \theta)I_0(\lambda)e^{-\int (\sum \alpha(\lambda)\rho(l) + \sigma_s^{ray}(\lambda)\rho_{ray}(l) + \sigma_s^{mie}(\lambda)\rho_r(l)) dl} \quad (2.24)$$

$a(\lambda, \theta)$  is the scattering efficiency. This gives the contribution of both types of scattering. The slant column density (SCD) is the total amount of absorber integrated along the light path as shown in figure 2.6 by the red lines. The light enters the atmosphere, and then is reflected off the earth's surface or scattered by particles or clouds back towards the satellite where the attenuated intensity is measured. It should be noted that the light path varies with different atmospheric conditions. On a cloudy day, the incoming solar radiation enters the cloud and then undergoes multiple scattering greatly increasing the light path (figure 2.7).

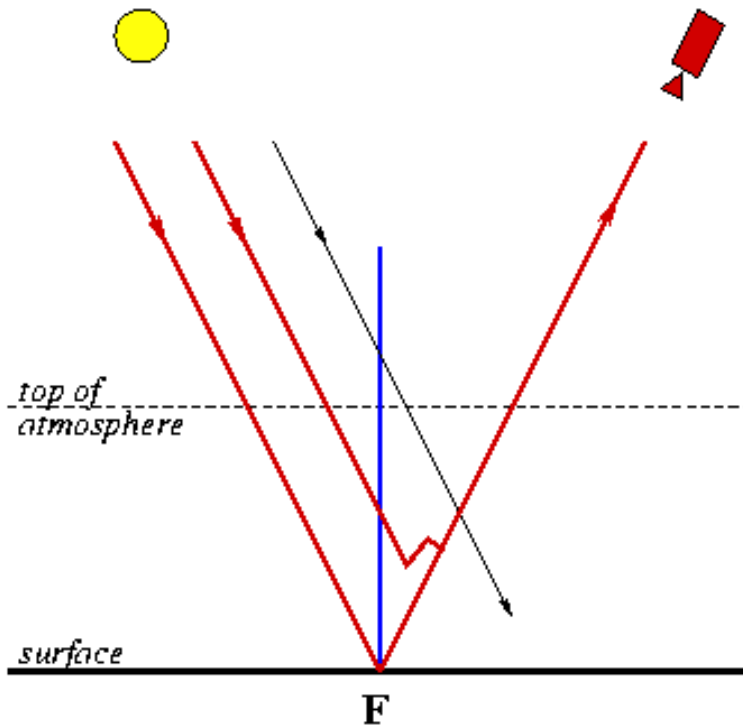
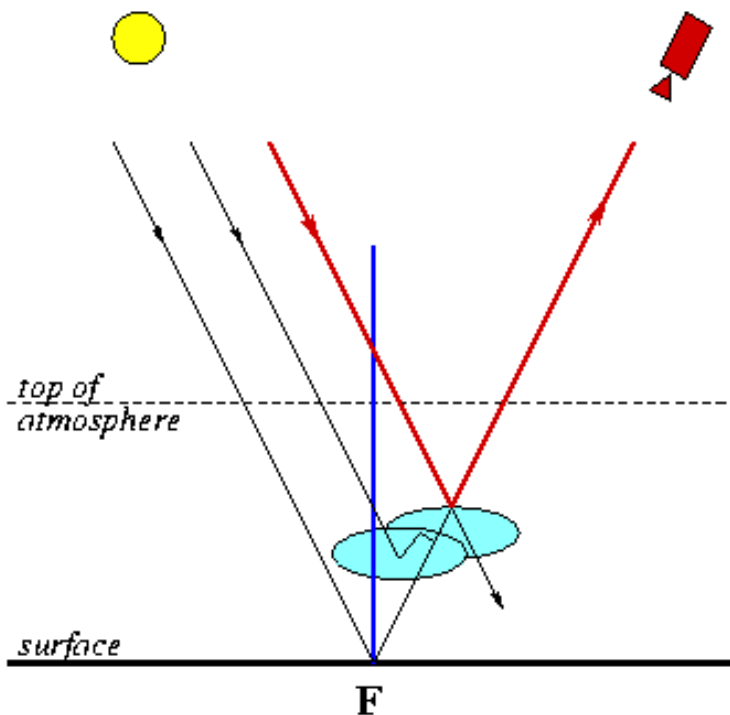


**Fig. 2.6.:** SCD represented by red line showing light path of incoming solar radiation on cloud free day. Source: <http://sacs.aeronomie.be/>



[http://sacs.aeronomie.be/info/scdvcd/scdclear\\_lr.gif](http://sacs.aeronomie.be/info/scdvcd/scdclear_lr.gif)

**Fig. 2.7.:** SCD represented by red line showing light path of incoming solar radiation on cloudy day. Source: <http://sacs.aeronomie.be/>

The DOAS equation is simplified using the SCD resulting in:

$$I(\lambda) = a(\lambda, \theta)I_0(\lambda)e^{-\sum \sigma(\lambda)SCD + \sigma_s^{ray}(\lambda)SCD_{ray} + \sigma_s^{mie}(\lambda)SCD_{mie}} \quad (2.25)$$

Since Raleigh and Mie scattering vary smoothly with wavelength, they are approximated with low order polynomials.

$$I(\lambda) = a(\lambda, \theta)I_0(\lambda)e^{-\sum \sigma(\lambda)SCD + \sum b_p \lambda^p} \quad (2.26)$$

The logarithm is taken resulting in a linear equation between the optical depth, a polynomial and the slant columns of the absorbers.

$$\ln(I(\lambda)/I_0(\lambda)) = -\sum \sigma(\lambda)SCD + \sum b_p \lambda^p \quad (2.27)$$

The slant columns are then calculated for many species by solving the equation at different wavelengths. In order to calculate the Vertical Column Density (VCD), represented by the blue line in figure 2.6, the Air Mass Factor is calculated. The AMF relies on several factors including viewing geometry and the vertical distribution of the absorber. The VCD is then the SCD/AMF (Source: Measurement Techniques in Environmental Physics 2006 by Dr. Andreas Richter).

$$VCD = \frac{SCD}{AMF} \quad (2.28)$$



# Outline and description

## 3.1 GOME-II satellite retrievals

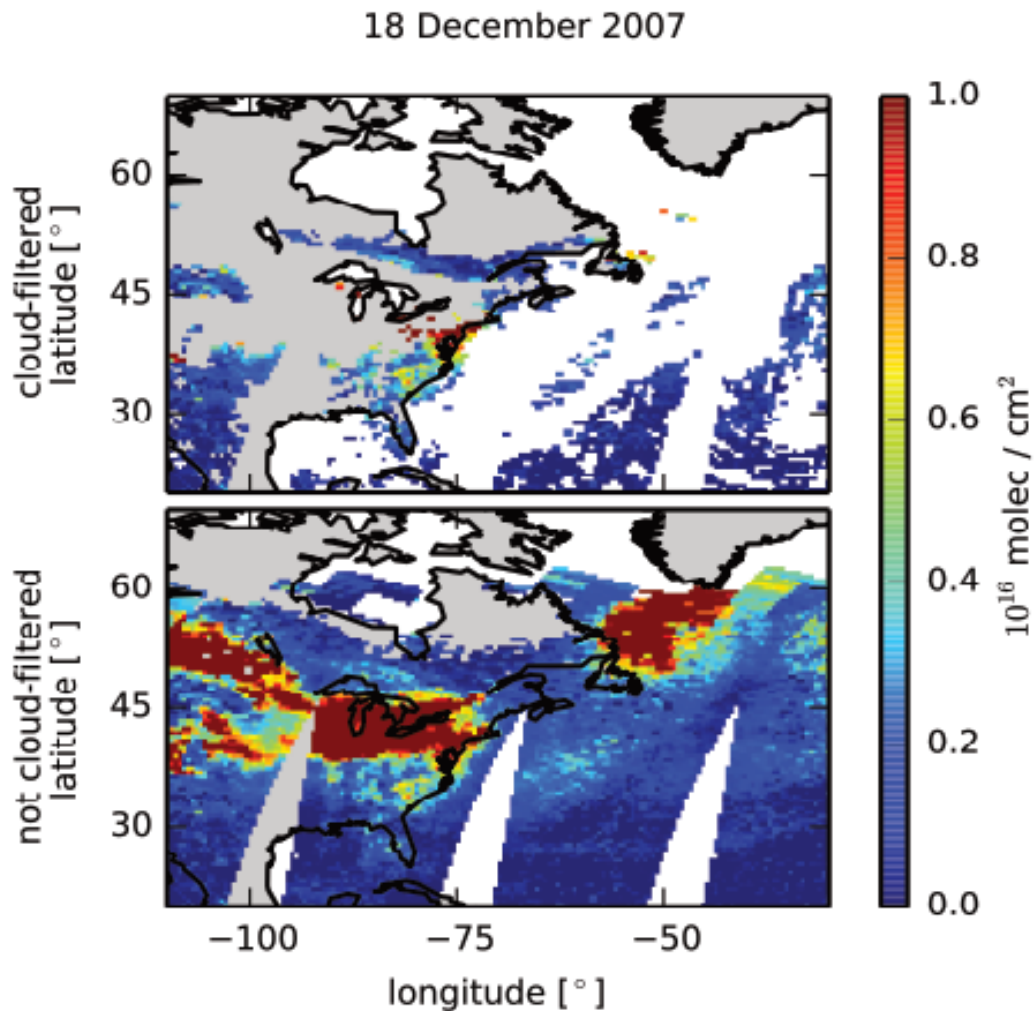
The Global Ozone Monitoring Experiment (GOME)-II is a spectrometer aboard the ESA METOP-A satellite. The spectrometer has a spectral range of 240 to 790 nm wavelength in four different channels. The instrument has a 4km x 40km field of view with a pixel width of 80x40 km<sup>2</sup> and a swath width of 1960 km obtained from a sweeping broom configuration. The METOP-A satellite is in a sun synchronous orbit and passes the equator at 09:30 local time on the descending node. The satellite orbits the earth 14 times a day and is able to obtain nearly global coverage in one day (Callies *et al.* [12]).

For this study, GOME-II tropospheric NO<sub>2</sub> VCD retrievals by Zien *et al.* [36] are used for model comparison. The satellite data uses a special AMF and does not have a cloud filter applied. Zien *et al.* [36] calculated the AMF using the SCIATRAN radiative transfer model for this project. For this study, we are only interested in the tropospheric VCD. A stratospheric correction was applied by Zien *et al.* [36] to the GOME-2 data. The stratospheric contribution was calculated using the B3dCTM chemical transport model. This stratospheric VCD column was converted to SCD and then subtracted from the total SCD.

$$VCD_{tropo} = \frac{SCD_{total} - (VCD_{strato} \cdot AMF_{strato})}{AMF_{tropo}} \quad (3.1)$$

Figure 3.1 shows the vertical column density with and without the cloud filter applied as an example for the date of December 18, 2007. The special air mass factor is applied because clouds alter the block AMF in several ways including increased cloud reflectivity due to the albedo effect, elongated light path inside the cloud due to multiple scattering, and little light penetrates through

the cloud and re transmits back to the satellite leading to a shielding effect. Zien *et al.* [36] assumed that NO<sub>2</sub> is homogeneously distributed throughout the cloud at a height of 3-5 km making it possible to measure the amount of NO<sub>2</sub> in the atmosphere even during cloudy events.



Zien *et al.* (2014)

**Fig. 3.1.:** Image showing NO<sub>2</sub> VCD with and without cloud filtering taken from Zien *et al.* [36]

## 3.2 Chemistry transport models

Two models are used for this study. These models are chosen as they are widely used in atmospheric research. The MACC-II Reanalysis model is a

global chemistry transport model while the WRF-Chem model is a regional high resolution model.

### 3.2.1 MACC-II

In Monitoring Atmospheric Composition and Climate (MACC)- Interim Implementation (II), a global CTM model combines ECMWF's IFS weather model with chemistry. Satellite and in-situ measurements are assimilated into the different MACC model runs and the models output global records of the distribution of trace gases. It also has the ability to output forecasts for reactive gases (Inness *et al.* [23]). Figure 3.2 shows the analysis process used in MACC-II. Satellite and other data along with estimates of fire and other emissions are input into the models and analyzed. The models then develop forecasts based on the initial inputs. The MACC-II models are run with different resolutions and chemistry schemes. In the following, MACC-II Reanalysis data is used which is based on MOZART chemistry. The atmospheric component of the MACC-II Reanalysis has a spectral resolution of T255L60 corresponding to  $0.7^\circ$  and 60 vertical levels while the chemistry model resolution is  $1.125^\circ \times 1.125^\circ$  (Antonakaki *et al.* [1]). MACC-II Reanalysis uses the MACCity global anthropogenic emissions inventory. The ECMWF-IFS is coupled to the MOZART chemistry.

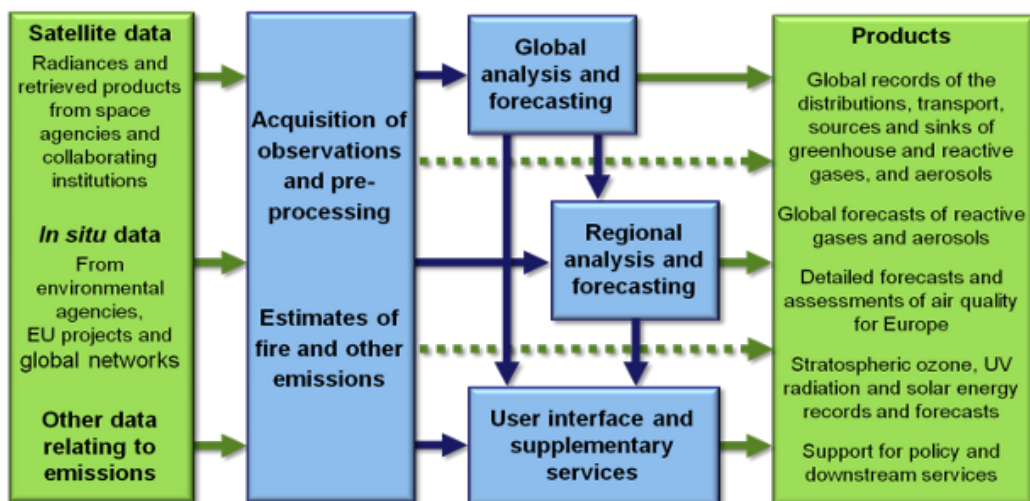


**Fig. 3.2.:** Flowchart depicting the analysis process of MACC-II. (<https://www.gmes-atmosphere.eu/about/project/>)

A model reanalysis is a data assimilation project which assimilates historical observational data spanning an extended period. The aim is to assimilate all previous data that may or may not have been available when the model was initially run.

### 3.2.2 WRF-Chem

The Weather Research and Forecasting coupled with chemistry (WRF-Chem) Model is an online, parallel computation model combining an atmospheric component and a chemistry component (Grell *et al.* [18]). Both components use the same transport scheme, the same horizontal and vertical grid, and the same physics. It also uses the same time step between the two components (Grell *et al.* [18]). WRF-Chem is a high resolution regional model which may allow for better performance in simulating LRT events. It can simulate NO<sub>2</sub> with a range of a few kilometers to 1000's of km making it a useful tool to study transport of NO<sub>2</sub> in weather systems. For this study, the model was run using MOZART-4/GEOS-5 chemistry for chemical boundary and initial conditions, NCEP 1° final analysis for meteorological boundary and initial conditions, and the RETRO emissions inventory for anthropogenic emissions. It was also run with accumulated chemistry diagnostic fields extended to include wet scavenging. Accumulated means starting from the initial time up until the time step being looked at. For example, the first output has all the data accumulated from simulation start until output time step. The model was run at two resolutions, 100km and 50km, in order to test whether agreement between model and satellite data improved with increased resolution. The domain was chosen in order to cover the entire area of interest shown in figure 3.3. The runs cover from September 30, 2010 to October 05, 2010 and has an output time step of three hours.

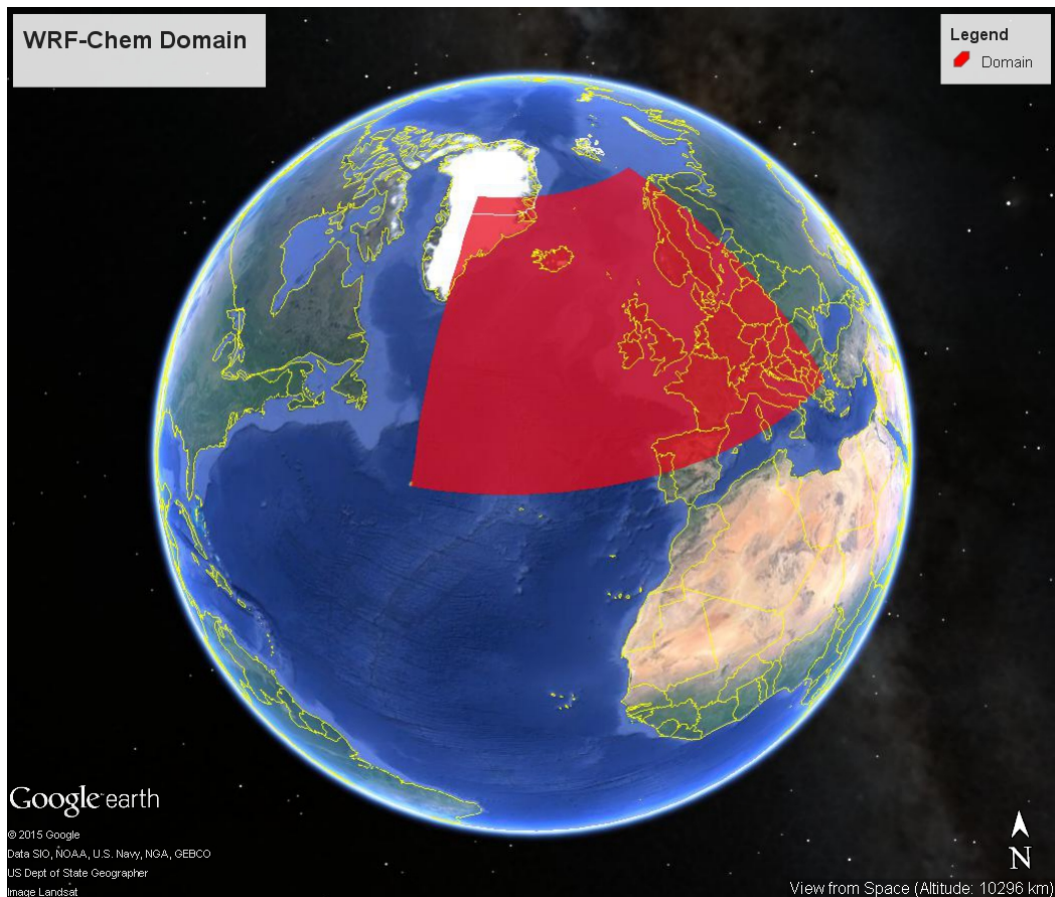


**Fig. 3.3.:** Domain of WRF-Chem model runs

The model version used is version 3.6.1.

### 3.3 Method of approach

The case investigated as well as the satellite data used is taken from the LRT dataset by Zien *et al.* [36]. A LRT event over the UK and central Europe spanning the dates of September 29, 2010 to October 05, 2010 is chosen for comparison between the models and the satellite data. The original MACC-II Reanalysis data for NO<sub>2</sub> is given in mole/mole for this study. It is processed using IDL to produce a data set of the total vertical column of NO<sub>2</sub> in molecules/cm<sup>2</sup> over the UK during the selected LRT event in order to

compare to the satellite NO<sub>2</sub> VCD data. This is accomplished by applying the equation

$$NO_2[\frac{molec}{cm^2}] = NO_2[\frac{mole}{mole}] \cdot (\frac{\Delta P \cdot N_a}{10^4 \cdot m_{dair} \cdot g}) \quad (3.2)$$

where  $\Delta P$  = pressure difference between model layer and interfaces.  $M_{dair}$  is the mass of dry air,  $g$  is gravity, and  $N_a$  is Avogadro's constant. The sum over all model levels then gives the total column of NO<sub>2</sub> in the atmosphere. The data is then plotted and saved for later comparison.

After a comparison of the MACC-II Reanalysis data and the satellite data, the WRF-Chem model will be evaluated against the same satellite data set in order to test performance of the model on LRT events of NO<sub>2</sub>. The WRF-Chem model outputs trace gas concentration in ppmv. The concentrations of trace gases are converted into  $\frac{molec}{cm^2}$  and combined into VCD in order to directly compare model results and satellite retrievals. The WRF-Chem model is also run at two different resolutions allowing us to investigate whether increased model resolution leads to better agreement with the satellite data. The role of the local weather systems for LRT at the time of measurement will also be investigated. We will also look into the sources (e.g. anthropogenic emissions, lightning) and sinks (e.g. HNO<sub>3</sub>, PAN) of NO<sub>2</sub> in order to analyze the transport of NO<sub>2</sub> by the cyclone in more detail.

# Results

For the comparisons of the satellite retrieval and model results, the days between September 30, 2010 and October 03, 2010 are used. These days cover the main part of the cyclone as it passes over the UK and Europe. All the model results are shown for 12:00 UTC, while the satellite observation time ranges between 10 and 14 UTC, over the area shown in the following satellite pictures. However, at the plume location (approximately 60° N) the satellite observation time is around 12 UTC. At this main area of interest, we expect the influence of the time difference between satellite and model to be negligible.

## 4.1 NO<sub>2</sub> Long Range Transport

The cyclone is the major influencing factor for this LRT event. The low pressure system moved towards the UK and the European mainland shown in figures 4.1a - 4.1c and caused a strong uplifting of the NO<sub>2</sub> into the free troposphere. Figures 4.1a - 4.1c show the Advanced Very High Resolution Radiometer (AVHRR) Dundee false color infrared satellite images. The false color image is a combination of three thermal infrared channels, one channel for red, green, and blue. The channels used by AVHRR are 1, 2, and 4 respectively and are used to produce the false color image. The colors represent:

- White or bluish white: Thick and cold clouds
- Light blue: Thin and cold clouds
- White or yellowish white: Mid-level clouds
- Yellow to sand brown: Low level clouds
- Yellowish white: Ice and snow

- Dark green: Land surface
- Dark blue: Ocean surface

these false color images show clouds as well, they are useful in order identify the location of fronts and hence vertical lifting for the NO<sub>2</sub> LRT event (AVHRR [3]).

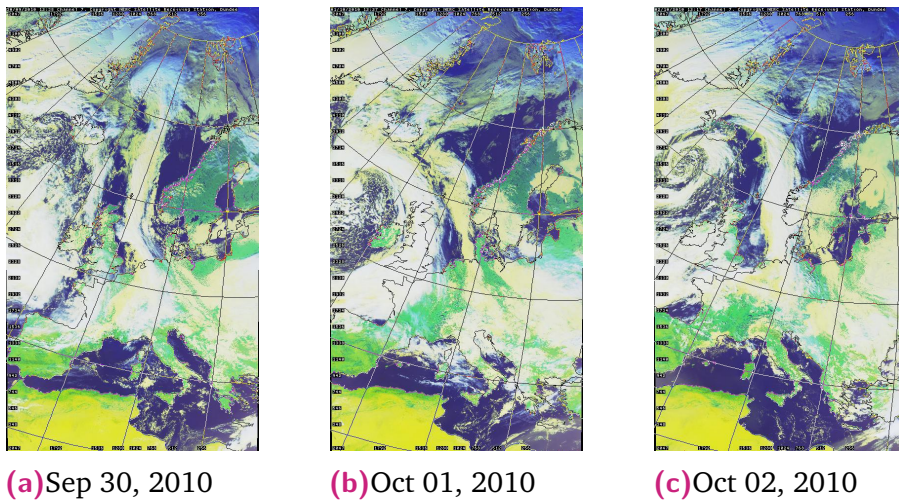


**Fig. 4.1.:** AVHRR satellite images showing the progression of the cyclone used for this study. (<http://www.sat.dundee.ac.uk/auth.html>)

When the GOME-2 satellite retrieval shown in figures 4.14a - 4.2c is compared to the AVHRR images, it is seen that the NO<sub>2</sub> tropospheric VCD retrieved follows the contours of the fronts in the cyclone. This is due to the fact that it was assumed in Zien *et al.* [36] that the trace gas is evenly distributed through the cloud at a height of 3-5 km but also because transport of trace gases happens along fronts. The figures show an elongated plume of NO<sub>2</sub> transported anticlockwise from Europe northwestward. The plume circles around the cyclone and is transported towards the center of the low pressure system. After October 02, the plume becomes less evident as the cyclone disperses.

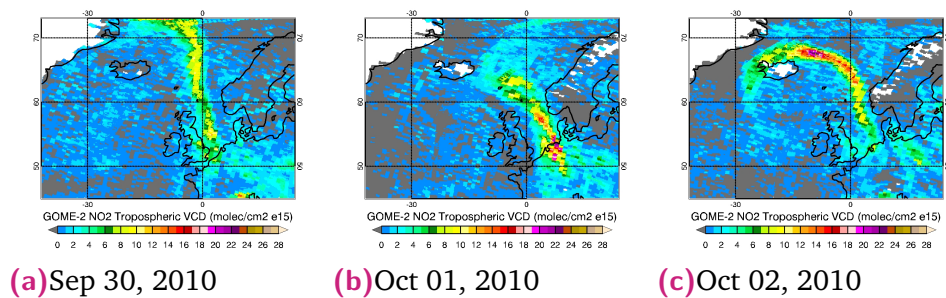
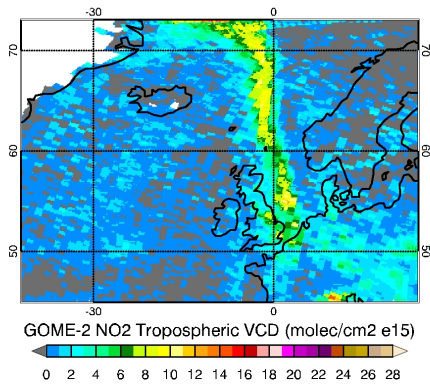


**Fig. 4.2.:** GOME-2 NO<sub>2</sub> tropospheric VCD (molec/cm<sup>2</sup> 10<sup>15</sup>).

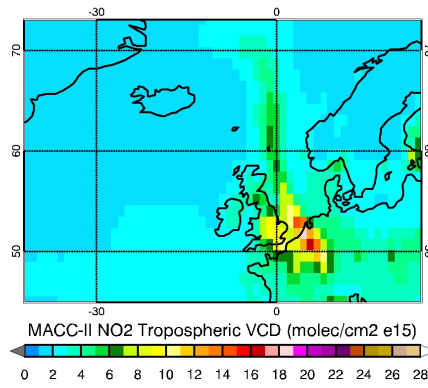
Figures 4.14a - 4.2c show the LRT of NO<sub>2</sub> from the emission regions in Europe through the cyclone towards the North Atlantic ocean and Iceland.

## 4.2 GOME-2 vs. MACC-II Reanalysis

In this section, the MACC-II Reanalysis simulations are compared to the GOME-2 retrievals of tropospheric NO<sub>2</sub> VCDs. The model shows a plume of NO<sub>2</sub> originating over the UK and northern Europe. The plume of NO<sub>2</sub> is transported northward and then northwestward as the cyclone passes over the region. The MACC-II model shows a higher background value over the ocean of about  $1-4 \times 10^{15}$  molec/cm<sup>2</sup>. A possible reason for the lower values represented in the GOME-2 measurements is that the satellite data represents the tropospheric excess column. This is the difference between the actual measurement and value determined in the reference region on the same day at the same latitude (Richter & Burrows [31]). The reference sector for these measurements is over the Pacific ocean. This can lead to an underestimation between  $4.5 \times 10^{14}$  at 48° and  $1.5 \times 10^{14}$  at 70° latitude according to estimates using the OSLO-CTM model (personal communication with Andreas Hilboll, IUP, University of Bremen).



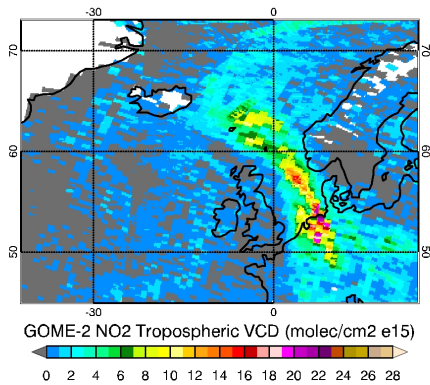
(a) GOME-2 Sep 30, 2010



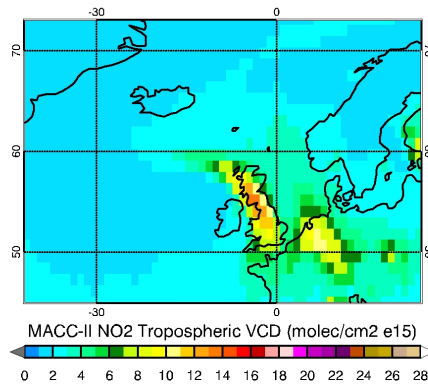
(b) MACC-II Reanalysis Sep 30, 2010

**Fig. 4.3.:** Comparison of GOME-2 NO<sub>2</sub> tropospheric VCD and MACC-II Reanalysis NO<sub>2</sub> tropospheric VCD (molec/cm<sup>2</sup> 10<sup>15</sup>).

On the first day of interest, we see a clear plume of NO<sub>2</sub> being emitted from the emission regions that is not shown in the GOME-2 data. This is due to the fact that the AMF for the GOME-2 data is most sensitive at 3-5km and therefore will underestimate NO<sub>2</sub> near the ground. The NO<sub>2</sub> plume is also not as strongly transported to the north on this day.



(a) GOME-2 Oct 01, 2010



(b) MACC-II Reanalysis Oct 01, 2010

**Fig. 4.4.:** Comparison of GOME-2 NO<sub>2</sub> tropospheric VCD and MACC-II Reanalysis NO<sub>2</sub> tropospheric VCD (molec/cm<sup>2</sup> 10<sup>15</sup>).

On October 01, the plume begins to circle around the cyclone. This is shown in both model and satellite data. The agreement between the model and satellite is not very good on Oct, 02. The main transport of NO<sub>2</sub> occurring in the model happens over the UK with much less transport happening over

Europe while the satellite shows all the transport coming from Europe with little to no readings over the UK due to the nature of the retrieval.

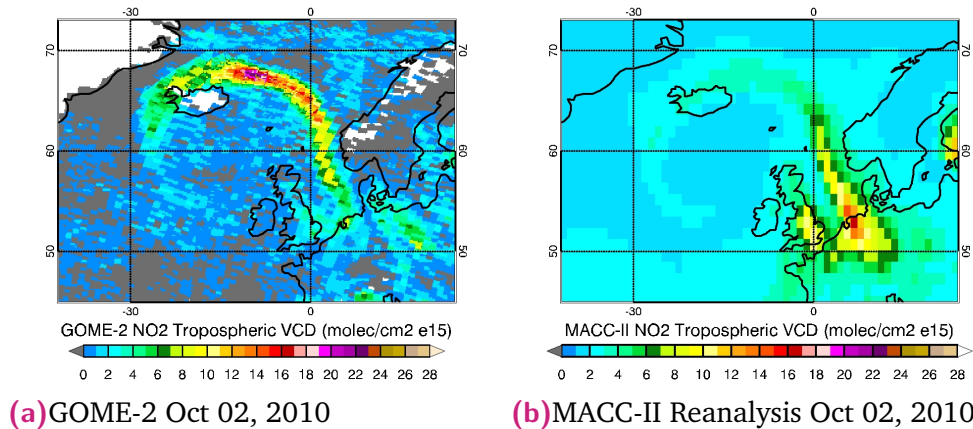


**Fig. 4.5.:** Comparison of GOME-2 NO<sub>2</sub> tropospheric VCD and MACC-II Reanalysis NO<sub>2</sub> tropospheric VCD (molec/cm<sup>2</sup> 10<sup>15</sup>).

October 02, is when the strongest part of the cyclone passes through the region. The satellite shows a clearly defined LRT of NO<sub>2</sub> through the cyclone towards the center of the system. The MACC-II model also shows transport but the strength of the transport northward is much lower than that of the satellite. This means that the VCD away from the emission region is underestimated by the model. The MACC-II model also has a lower spatial resolution than the GOME-2 data. This leads to a coarser spatial resolution and therefore less agreement with the satellite.

## 4.3 MACC-II Reanalysis vs. WRF-Chem

### 100km

The next step is to compare the MACC-II results with the 100km resolution run of the WRF-Chem model. This is done because the 100km run is much closer in resolution to the MACC-II Reanalysis model than the MACC-II model is to the satellite retrieval. Hence, we can see if model performance improves with higher resolution. The resolution of the MACC-II model is 1.125° x 1.125° or about 70km in the longitudinal direction and about 125km in the

latitudinal direction in the center of the region of interest. For all days, the background values over the ocean for the WRF-Chem model are lower when compared to the MACC-II model.

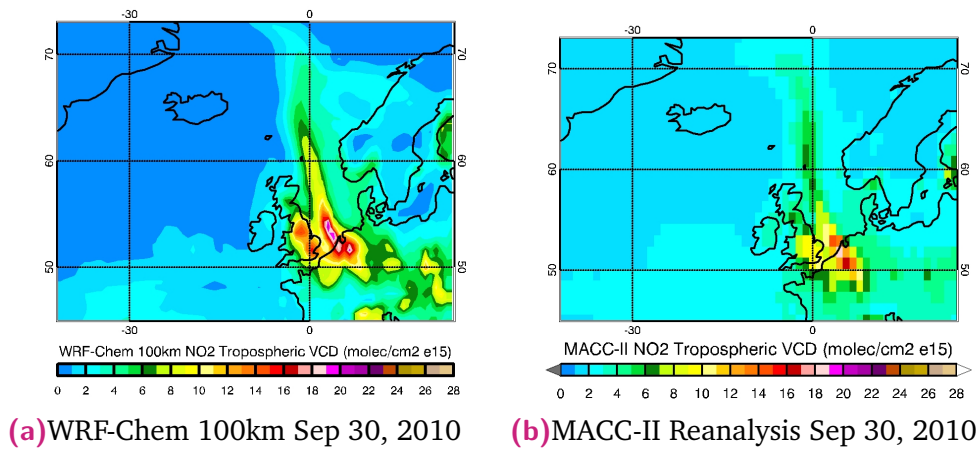


**Fig. 4.6.:** Comparison of WRF-Chem 100 km resolution NO<sub>2</sub> tropospheric VCD and MACC-II Reanalysis NO<sub>2</sub> tropospheric VCD (molec/cm<sup>2</sup> 10<sup>15</sup>).

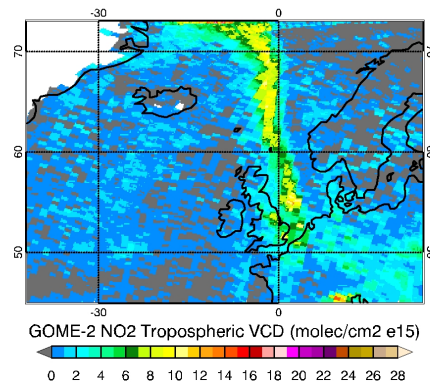


**Fig. 4.7.:** GOME-2 Satellite retrieval NO<sub>2</sub> tropospheric VCD Sep 30, 2010 (molec/cm<sup>2</sup> 10<sup>15</sup>).

The figures show that the spatial similarities between the two models are very strong. On September 30, both models show the transport of NO<sub>2</sub> to the north. The WRF-Chem model has higher values in the plume, while at the same time showing lower values over the ocean. The VCD values are also higher at the emission sources in the WRF-Chem model. When comparing both models at this resolution to the GOME-2 data, we see that the WRF-Chem model better represents the transport of NO<sub>2</sub>.

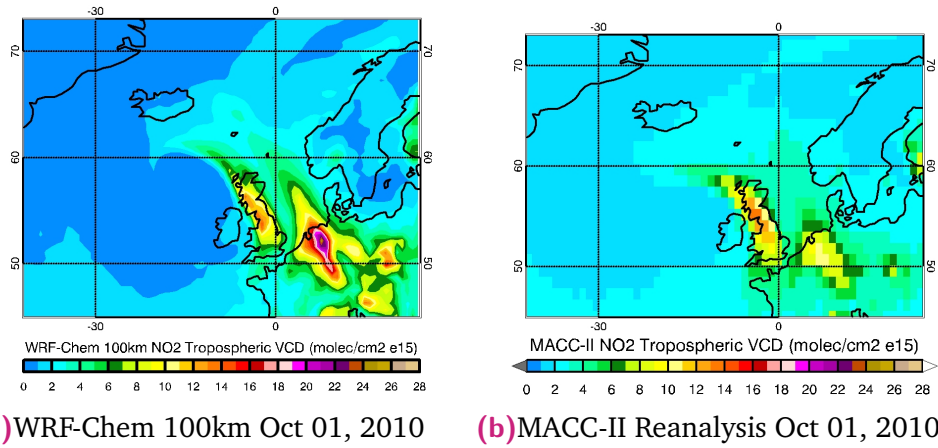


**Fig. 4.8.:** Comparison of WRF-Chem 100 km resolution NO<sub>2</sub> tropospheric VCD and MACC-II Reanalysis NO<sub>2</sub> tropospheric VCD (molec/cm<sup>2</sup> 10<sup>15</sup>).

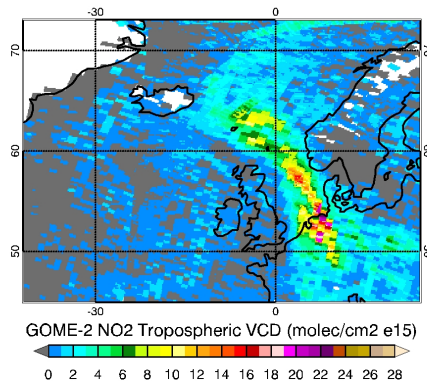


**Fig. 4.9.:** GOME-2 Satellite retrieval NO<sub>2</sub> tropospheric VCD Oct 01, 2010 (molec/cm<sup>2</sup> 10<sup>15</sup>).

The 1st and 2nd of October also shows strong spatial similarity. On October 02, the NO<sub>2</sub> plume is seen clearly being transported further towards the center of the cyclone than the MACC-II model NO<sub>2</sub> plume. There are in principle several reasons for this. One possible reason for the difference could be that the contrast in values between the plume over the ocean background values differs between the models. If the values were lower over the ocean for the MACC-II Reanalysis model, then the similarities would be stronger. Another reason could be related to differences in chemistry settings and differences in emissions and the representation of the transport of NO<sub>2</sub> out of the boundary layer. All these factors can lead to differences in the models.

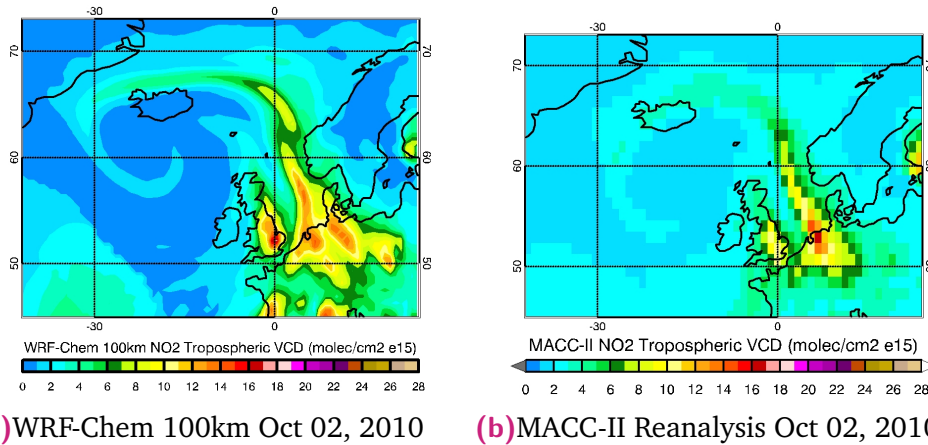


**Fig. 4.10.:** Comparison of WRF-Chem 100 km resolution NO<sub>2</sub> tropospheric VCD and MACC-II Reanalysis NO<sub>2</sub> tropospheric VCD (molec/cm<sup>2</sup> 10<sup>15</sup>).

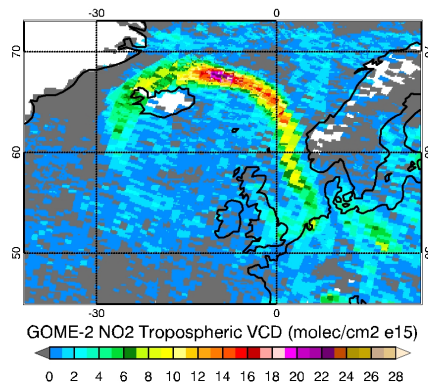


**Fig. 4.11.:** GOME-2 Satellite retrieval NO<sub>2</sub> tropospheric VCD Oct 02, 2010 (molec/cm<sup>2</sup> 10<sup>15</sup>).

When comparing the WRF-Chem 100km resolution run and the MACC-II Reanalysis directly with the GOME-2 retrieval, we see that the NO<sub>2</sub> is not being transported as far in the cyclone. We also see that the plume is wider for both models at this resolution than the satellite.

## 4.4 GOME-2 vs. WRF-Chem 50km

Increasing the resolution of the WRF-Chem model leads to better spatial similarities between the model and the satellite retrieval. The WRF-Chem model was run at 50km x 50km while the satellite pixel size is 80km x 40km. We still see the emission regions in the model simulated values that are

not shown in the satellite, but but the satellite retrieval is not sensitive to emissions close to the ground so this is expected. The shape of the plume represented by the model matches much more closely to the satellite than the MACC-II Reanalysis model does. This is due in part to the closer resolution between the model and satellite.

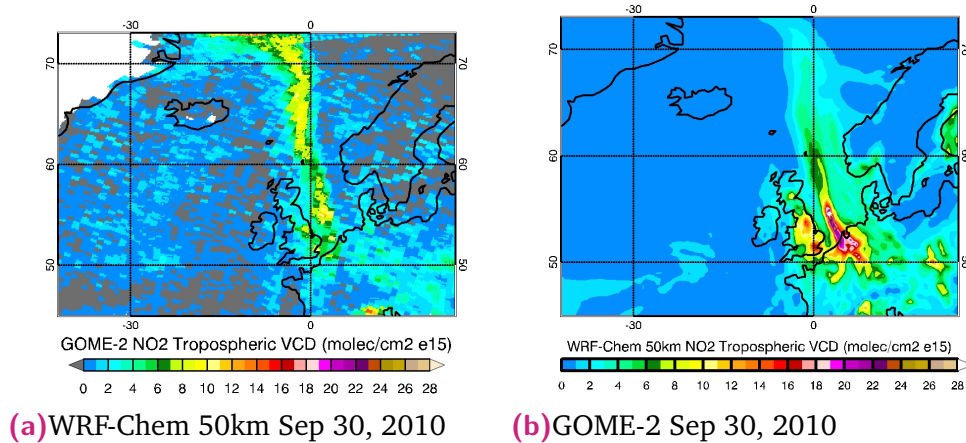


**Fig. 4.12.:** Comparison of WRF-Chem 50 km resolution  $\text{NO}_2$  tropospheric VCD and GOME-2  $\text{NO}_2$  tropospheric VCD ( $\text{molec}/\text{cm}^2 10^{15}$ ).

The model shows northward transport of  $\text{NO}_2$  on September 30, but the  $\text{NO}_2$  in the model still does not progress as far as the  $\text{NO}_2$  in the satellite.

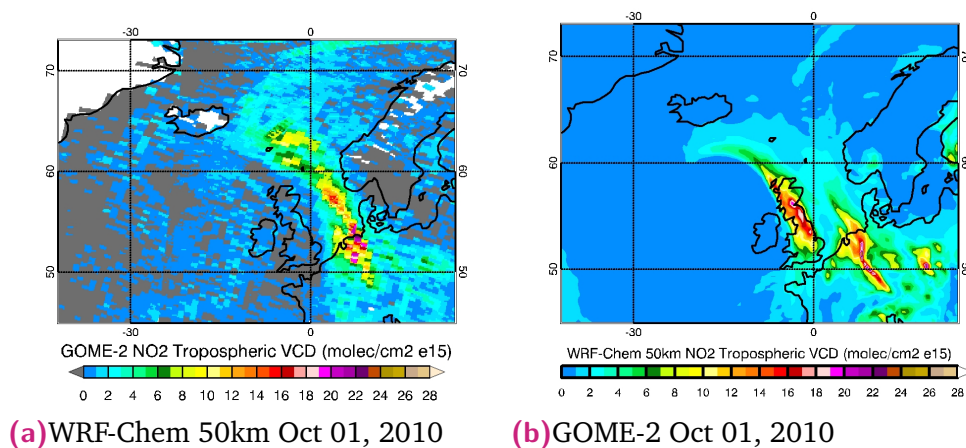


**Fig. 4.13.:** Comparison of WRF-Chem 50 km resolution  $\text{NO}_2$  tropospheric VCD and GOME-2  $\text{NO}_2$  tropospheric VCD ( $\text{molec}/\text{cm}^2 10^{15}$ ).

The spatial agreement breaks down again on October 01. A majority of the transport is shown coming from the UK in the model while the  $\text{NO}_2$  transport

is shown coming from Europe in the satellite data. This could partly be due to the nature of the retrieval over the UK, since it is close to the emission region. The GOME-2 data in fact shows little to no  $\text{NO}_2$  in the region indicated by the model.

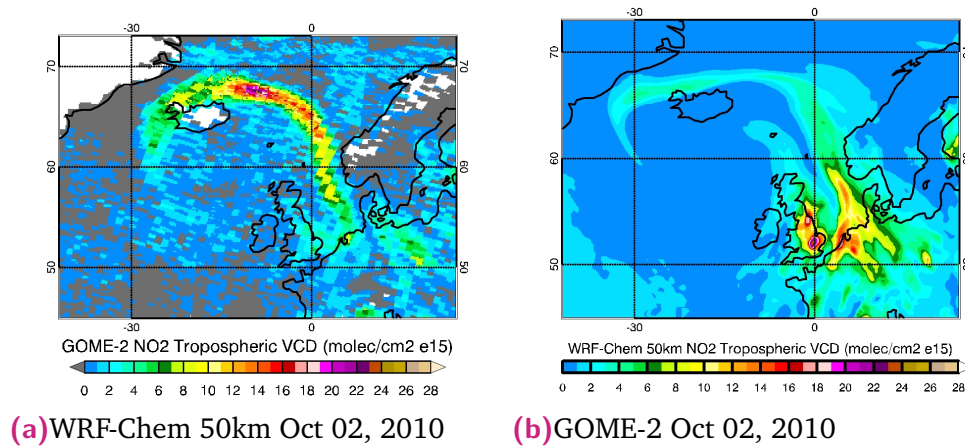


**Fig. 4.14.:** Comparison of WRF-Chem 50 km resolution  $\text{NO}_2$  tropospheric VCD and GOME-2  $\text{NO}_2$  tropospheric VCD ( $\text{molec}/\text{cm}^2 \cdot 10^{15}$ ).

The model regains spatial similarities on the 2nd of October. The  $\text{NO}_2$  plume extends further north and then is transported through the cyclone towards the low pressure center. While the transport is not as strong as for the GOME-2 data, the WRF-Chem model shows more transport than the MACC-II model. As will be shown in section 4.5, a major reason that the  $\text{NO}_2$  is not being transported in the WRF-Chem model is that the  $\text{NO}_2$  is being converted into  $\text{HNO}_3$  in the boundary layer before it is able to make it into the free troposphere and be transported long distances.

## 4.5 WRF-Chem chemistry diagnostics

Using chemical diagnostic fields and other trace gases output from the WRF-Chem model, it is possible to determine the chemical conversion and transport of the  $\text{NO}_2$  during the LRT event. We are able to see the  $\text{NO}_2$  converted into other species. These species can then act as a sink or reservoir of  $\text{NO}_2$ .

## 4.5.1 NO<sub>2</sub> Chemical Conversion

NO<sub>2</sub> is an extremely reactive trace gas. In the boundary layer, it is quickly converted into other species. While the satellite retrieval shows a significant amount of NO<sub>2</sub> being transported in the cyclone away from the emission regions, the models show much less NO<sub>2</sub> being transported. At least for the WRF-Chem model, a reasonable explanation for this is the conversion of NO<sub>2</sub> to HNO<sub>3</sub>. This conversion is fast in the model preventing the NO<sub>2</sub> from escaping into the free troposphere. In figures 4.15a and 4.15b we see the accumulated chemical conversion of HNO<sub>3</sub> and NO<sub>2</sub>. Another reason could be that the emissions of NO<sub>x</sub> are not large enough. This means that the emission inventories used could be underestimating the emissions.

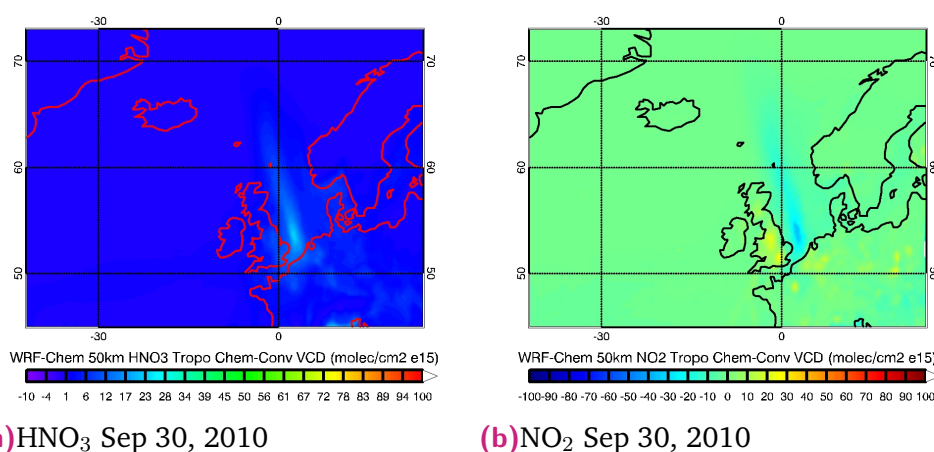


**Fig. 4.15.:** Comparison of accumulated chemical conversion fields of HNO<sub>3</sub> and NO<sub>2</sub> (molec/cm<sup>2</sup> 10<sup>15</sup>).

As the storm progresses, almost all of the NO<sub>2</sub> is being converted into HNO<sub>3</sub> as seen in figures 4.16a - 4.17b. The model shows that where there is a loss of around 50 molec/cm<sup>2</sup> of NO<sub>2</sub>, there is also a gain of around 50 molec/cm<sup>2</sup> HNO<sub>3</sub> in the same area. This inhibits the transport of NO<sub>2</sub>.

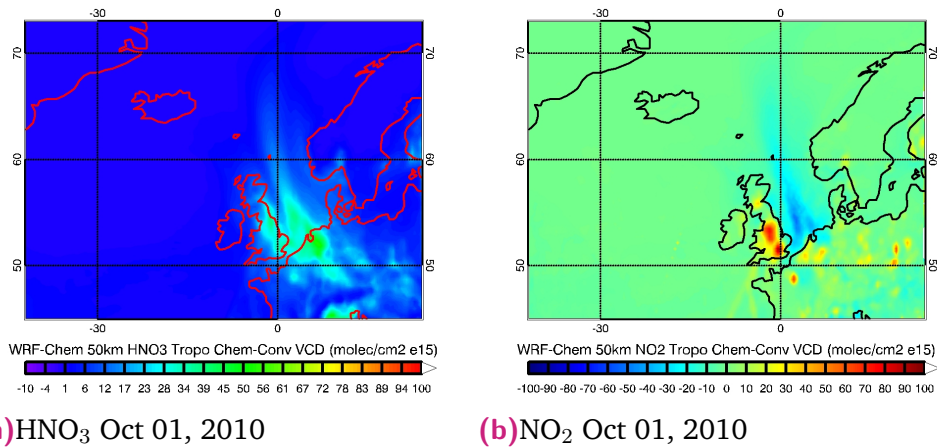


**Fig. 4.16.:** Comparison of accumulated chemical conversion fields of HNO<sub>3</sub> and NO<sub>2</sub> (molec/cm<sup>2</sup> 10<sup>15</sup>).

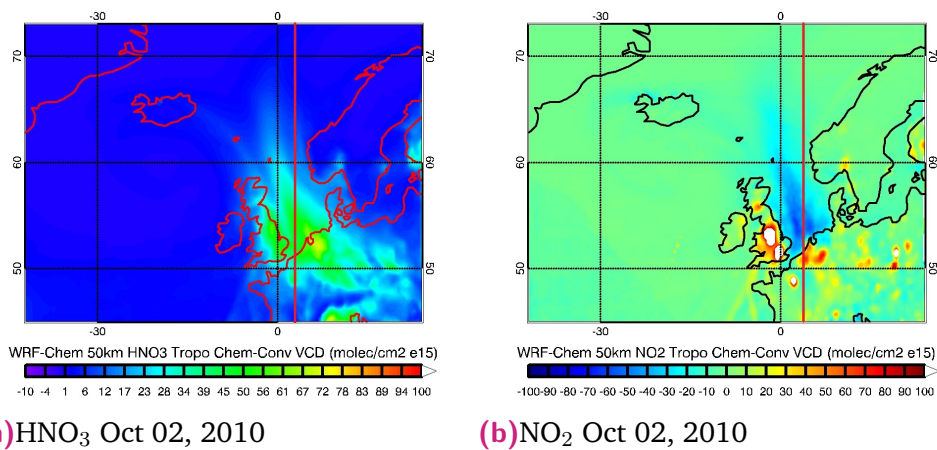
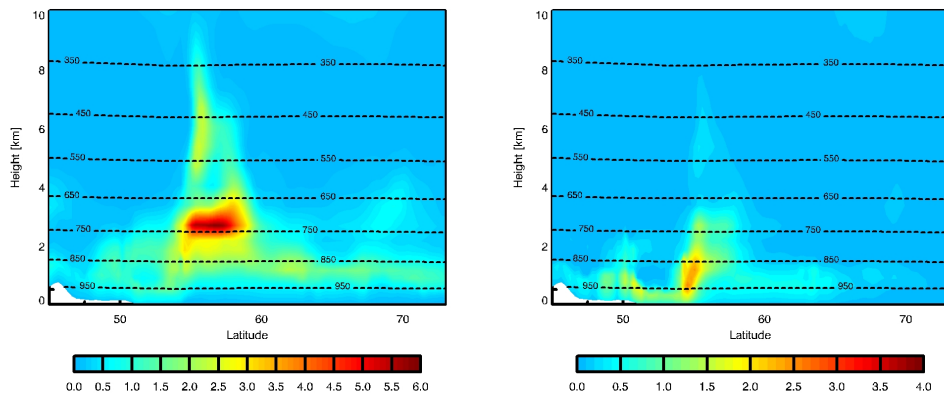


**Fig. 4.17.:** Comparison of accumulated chemical conversion fields of HNO<sub>3</sub> and NO<sub>2</sub> (molec/cm<sup>2</sup> 10<sup>15</sup>).

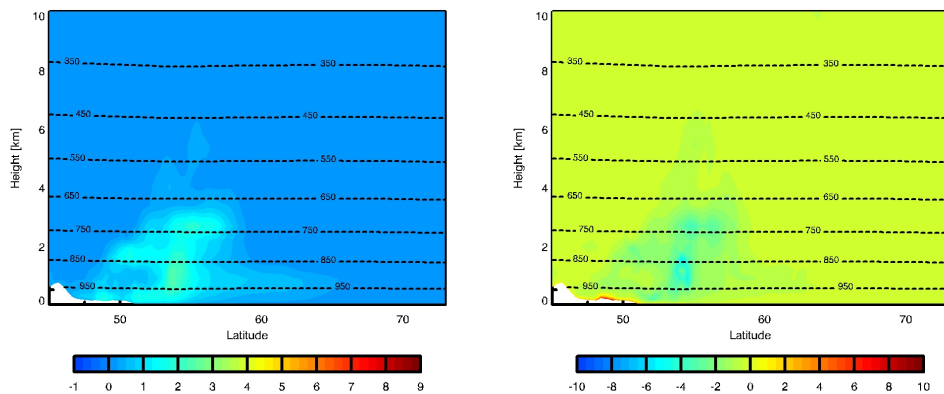
The inhibition of transport of NO<sub>2</sub> is especially apparent when viewing the vertical profiles of the trace gases. The red lines in figures 4.17a and 4.17b show the region that the vertical profile taken. This region was chosen in order to see the transport of trace gases from the emission region northward in the cyclone. Vertical profiles for different time steps were plotted at 2° longitude in order to see the transport of trace gases from the emission region northward. Figures 4.18a and 4.18b show the HNO<sub>3</sub> and NO<sub>2</sub> vertical profiles respectively. On September 30, the day before the storm arrives, a large portion of the NO<sub>2</sub> is converted into HNO<sub>3</sub> near the ground (4.19a and

4.19b). It is shown in the figures that most of the NO<sub>2</sub> stays near the ground while the HNO<sub>3</sub> is lifted up.



(a) HNO<sub>3</sub> vertical profile Sep 30, 2010 (b) NO<sub>2</sub> vertical profile Sep 30, 2010

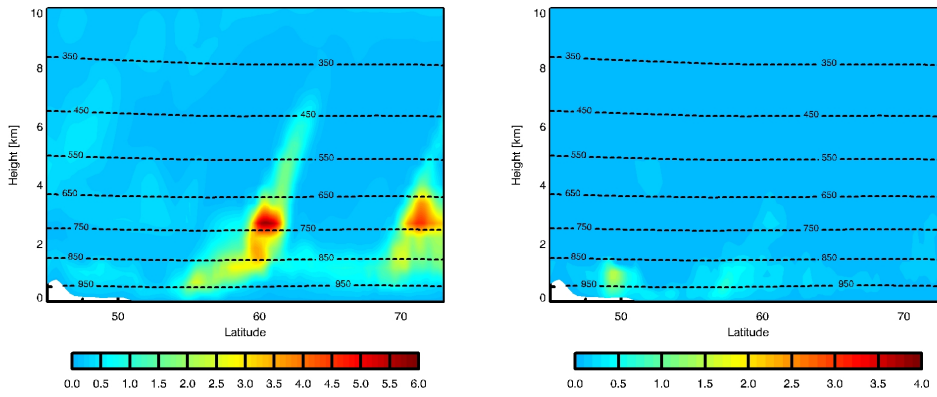
**Fig. 4.18.:** Vertical profile of HNO<sub>3</sub> and NO<sub>2</sub> showing transport into the troposphere. (molec/cm<sup>3</sup> 10<sup>15</sup>).



(a) chem HNO<sub>3</sub> vert prof 09-30 (b) chem NO<sub>2</sub> vert prof 09-30

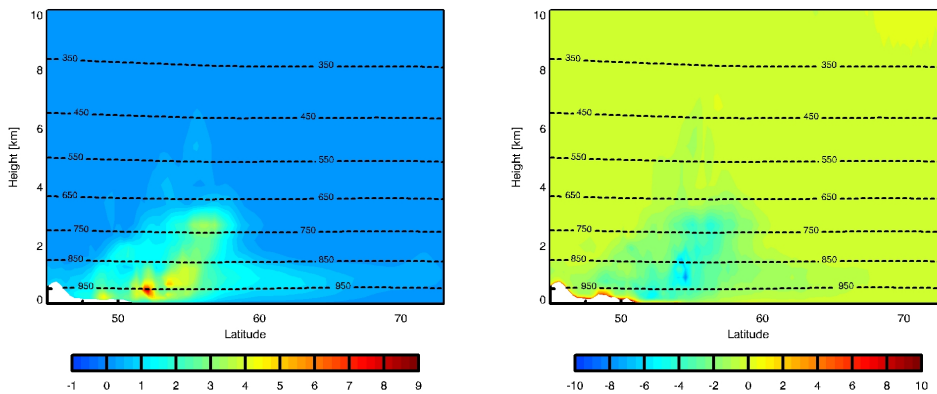
**Fig. 4.19.:** Accumulated chemical conversion vertical profile of HNO<sub>3</sub> and NO<sub>2</sub> (molec/cm<sup>3</sup> 10<sup>15</sup>).

As the cyclone begins to pass over the UK and Northern Europe on October 01, most of the NO<sub>2</sub> is still being converted into HNO<sub>3</sub> near the ground as shown by figures 4.21a - 4.21b, but the HNO<sub>3</sub> is being lifted vertically higher into the troposphere and transported northward with the storm.



(a)  $\text{HNO}_3$  vertical profile Oct 01, 2010 (b)  $\text{NO}_2$  vertical profile Oct 01, 2010

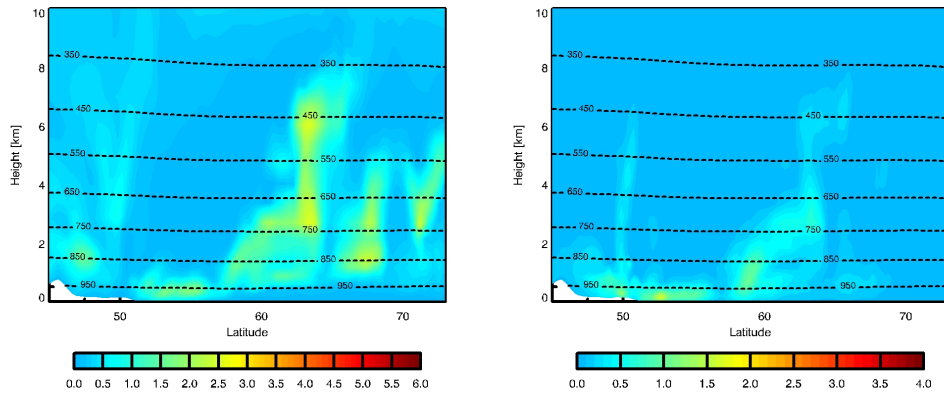
**Fig. 4.20.:** Vertical profile of  $\text{HNO}_3$  and  $\text{NO}_2$  showing transport into the troposphere. (molec/cm<sup>3</sup> 10<sup>15</sup>).



(a) chem  $\text{HNO}_3$  vert prof Oct 01, 2010 (b) chem  $\text{NO}_2$  vert prof Oct 01, 2010

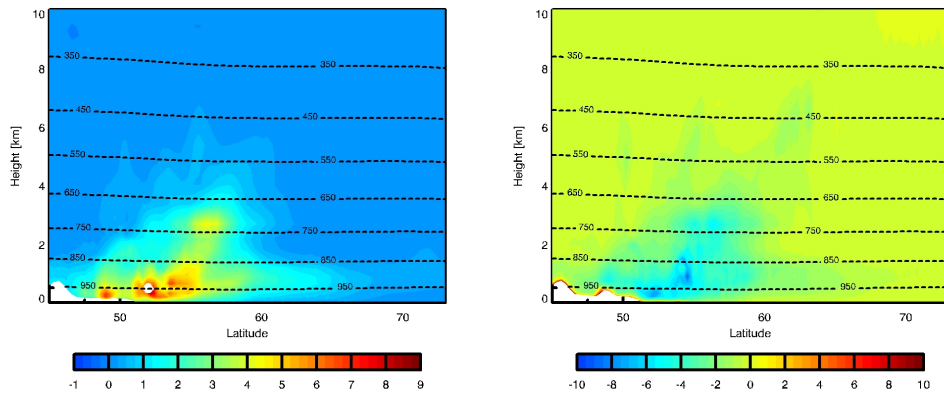
**Fig. 4.21.:** Accumulated chemical conversion vertical profile of  $\text{HNO}_3$  and  $\text{NO}_2$  (molec/cm<sup>3</sup> 10<sup>15</sup>).

As the cyclone intensifies over the region on October 02, the  $\text{NO}_2$  starts to be transported vertically as well as the  $\text{HNO}_3$  shown by figures 4.22a - 4.22b. This is due to the strong upwelling forces associated with the passing of the cold front in the cyclone.



(a) HNO<sub>3</sub> vertical profile Oct 02, 2010 (b) NO<sub>2</sub> vertical profile Oct 02, 2010

**Fig. 4.22.:** Vertical profile of HNO<sub>3</sub> and NO<sub>2</sub> showing transport into the troposphere. (molec/cm<sup>3</sup> 10<sup>15</sup>).



(a) chem HNO<sub>3</sub> vert prof Oct 02, 2010 (b) chem NO<sub>2</sub> vert prof Oct 02, 2010

**Fig. 4.23.:** Accumulated chemical conversion vertical profile of HNO<sub>3</sub> and NO<sub>2</sub> (molec/cm<sup>3</sup> 10<sup>15</sup>).

These results show that the NO<sub>2</sub> is being converted into HNO<sub>3</sub> before it is able to exit the boundary layer and be transported long distances. Conversion rates in the WRF-Chem model give a reasonable explanation of why the plume NO<sub>2</sub> VCD values in the WRF-Chem model are lower than that of the GOME-2 data. However, uncertainties regarding emission values, and boundary layer physics also apply

## 4.5.2 HNO<sub>3</sub> Wet Scavenging

As we have seen in the previous section, HNO<sub>3</sub> is the primary sink of NO<sub>2</sub> in this LRT event. Moreover, HNO<sub>3</sub> is highly susceptible to wet scavenging

by rain. Since large amounts of rain are expected to accompany a cyclone, it is then expected that the  $\text{NO}_2$  is converted into  $\text{HNO}_3$  and then washed out from the atmosphere along with the fronts. The model was extended to include chemistry diagnostics of wet scavenging and it shows that a large portion of the  $\text{HNO}_3$  that was formed from  $\text{NO}_2$  is scavenged out.

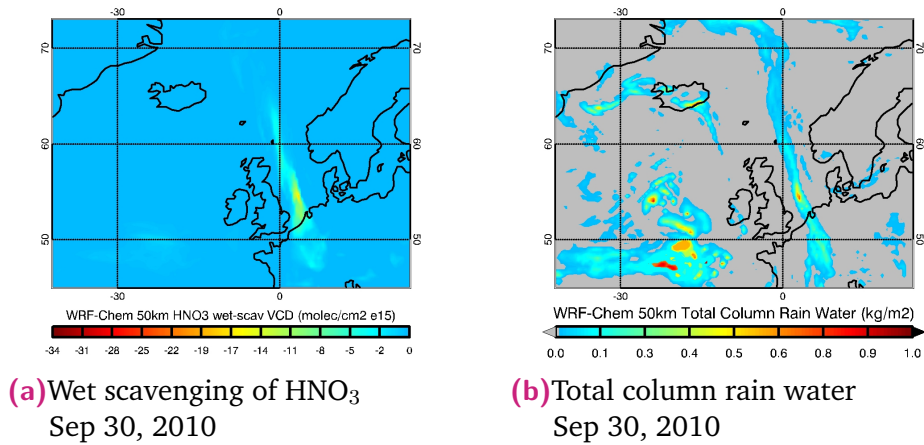


**Fig. 4.24.:** Comparison of  $\text{HNO}_3$  accumulated wet scavenging ( $\text{molec}/\text{cm}^2 \cdot 10^{15}$ ) and total column rain water ( $\text{kg}/\text{m}^2$ ).

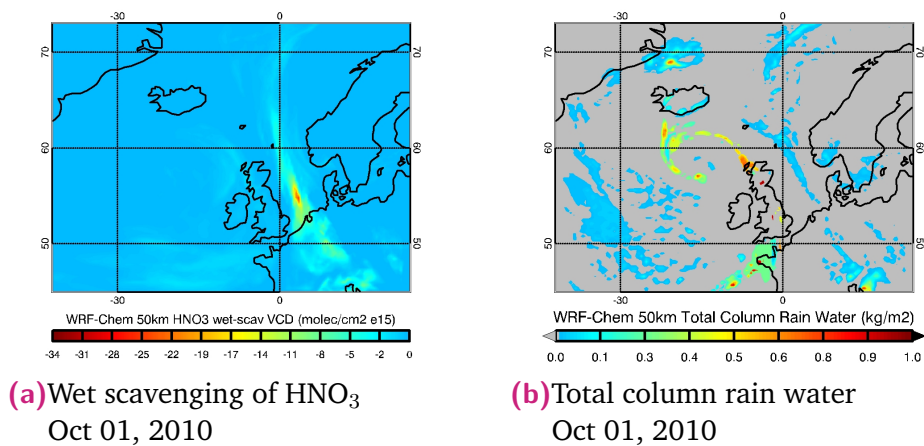


**Fig. 4.25.:** Comparison of  $\text{HNO}_3$  accumulated wet scavenging ( $\text{molec}/\text{cm}^2 \cdot 10^{15}$ ) and total column rain water ( $\text{kg}/\text{m}^2$ ).

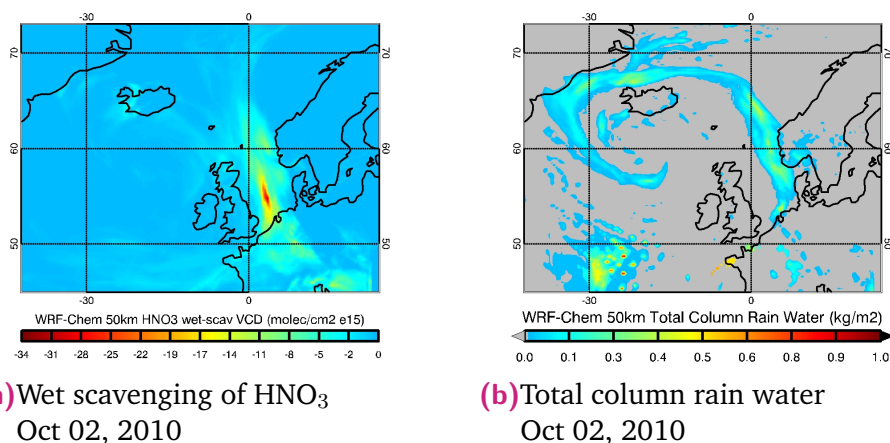


**Fig. 4.26.:** Comparison of  $\text{HNO}_3$  accumulated wet scavenging ( $\text{molec}/\text{cm}^2 \cdot 10^{15}$ ) and total column rain water ( $\text{kg}/\text{m}^2$ ).

Figures 4.24a, 4.25a, and 4.26a show the accumulated wet scavenging of  $\text{HNO}_3$  as computed by the model. Since wet scavenging is always a loss process, all values are negative. When compared side by side with rain water computed by the model shown by figures 4.24b, 4.25b, and 4.26b, we can see that the scavenging happens in areas associated with rainfall. Especially in cyclones,  $\text{HNO}_3$  is an efficient sink for  $\text{NO}_2$

### 4.5.3 $\text{HNO}_3$ Transport

$\text{HNO}_3$  is typically formed when  $\text{NO}_2$  and OH react. This reaction plays a role in the formation and transport of  $\text{HNO}_3$  in cyclones.

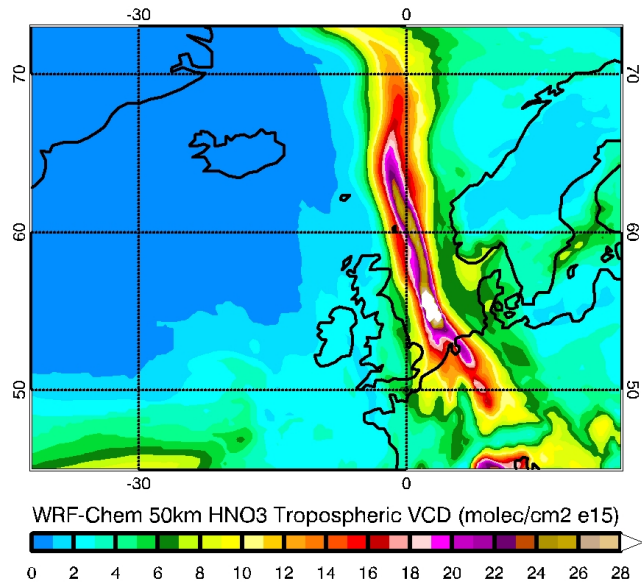


**Fig. 4.27.:** HNO<sub>3</sub> tropospheric VCD (molec/cm<sup>2</sup> 10<sup>15</sup>) Sep 30, 2010.

On September 30 (figure 4.27), a large amount of HNO<sub>3</sub> is seen being transported from the emission region in Northern Europe northward along the front. This shape is characteristic of transport along the warm conveyor belt between the two fronts of the cyclone.

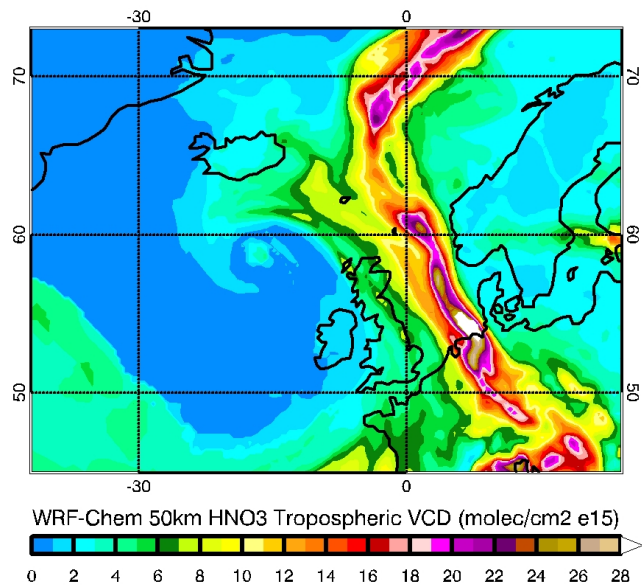


**Fig. 4.28.:** HNO<sub>3</sub> tropospheric VCD (molec/cm<sup>2</sup> 10<sup>15</sup>) Oct 01, 2010.

While most of the  $\text{HNO}_3$  continues to follow the warm conveyor northward on October 01, some of the  $\text{HNO}_3$  starts to turn westward toward the low pressure center.

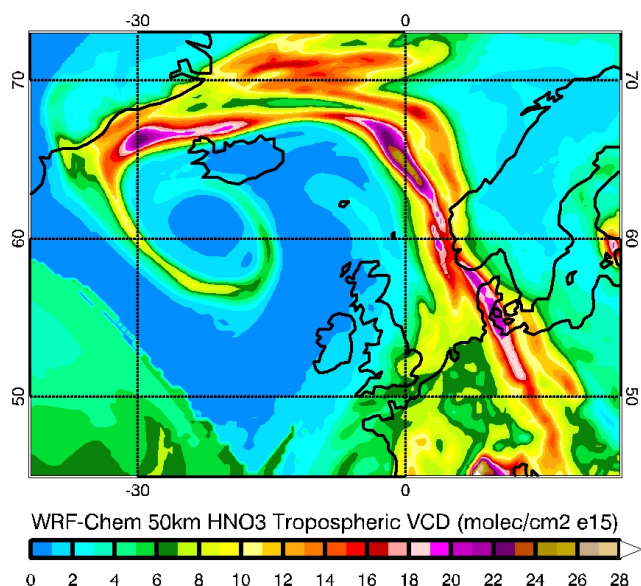


**Fig. 4.29.:**  $\text{HNO}_3$  tropospheric VCD ( $\text{molec}/\text{cm}^2 \cdot 10^{15}$ ) Oct 02, 2010.

On October 02, a majority of the  $\text{HNO}_3$  has started to move in an anticlockwise manner following the contours of the cyclone. These figures show that the  $\text{HNO}_3$  is being efficiently transported inside the cyclone and along the fronts. We saw in the previous section that most of the  $\text{HNO}_3$  formed from the conversion from  $\text{NO}_2$  was being wet scavenged out. This means that a large amount of  $\text{HNO}_3$  is being emitted and formed in parallel to the conversion from  $\text{NO}_2$ .

#### 4.5.4 PAN Transport

PAN is a reservoir for  $\text{NO}_2$ . The creation and destruction of PAN is also temperature dependent making the transport of the trace gas easy in LRT events. Since most of the  $\text{NO}_2$  is being converted into  $\text{HNO}_3$  according to the model, the amount of PAN being produced is negligible in comparison.

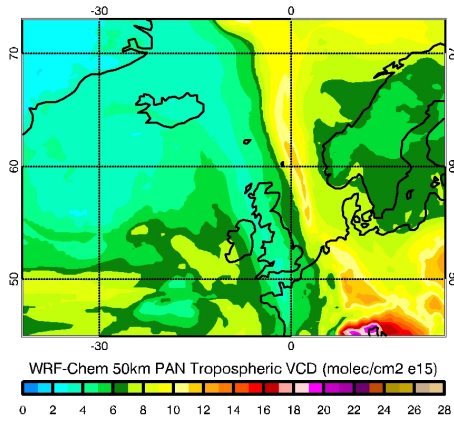


**Fig. 4.30.:** PAN tropospheric VCD (molec/cm<sup>2</sup> 10<sup>15</sup>) Sep 30, 2010

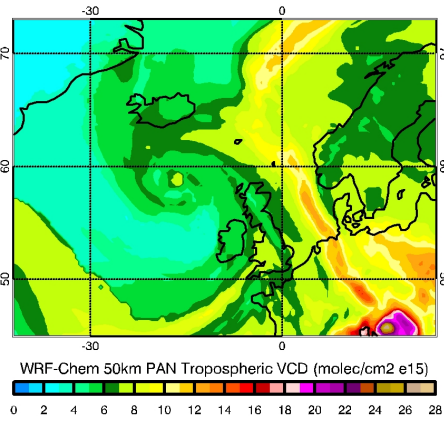


**Fig. 4.31.:** PAN tropospheric VCD (molec/cm<sup>2</sup> 10<sup>15</sup>) Oct 01, 2010

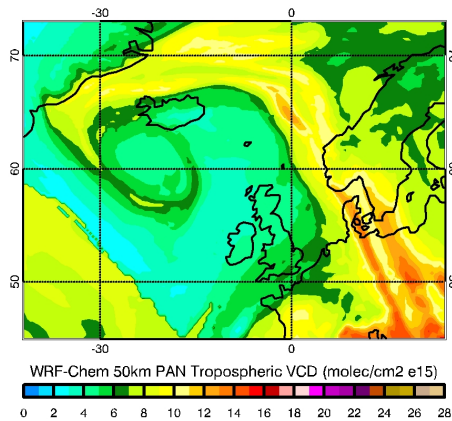


**Fig. 4.32.:** PAN tropospheric VCD (molec/cm<sup>2</sup> 10<sup>15</sup>) Oct 02, 2010

The model shows a large amount of transport of PAN during the cyclone. Similar to the transport of HNO<sub>3</sub>, PAN follows the warm conveyor belt on September 01. It is then transported with the cyclone in the anticlockwise direction towards the low pressure center. A large difference between PAN and the other trace gasses is that the emission region is further south than that of NO<sub>2</sub> or HNO<sub>3</sub>. This means that a majority of the PAN that is transported in the cyclone is coming from a separate emission source. We showed that almost all of the NO<sub>2</sub> being emitted was converting into HNO<sub>3</sub>. This left very little NO<sub>2</sub> to convert into PAN. The model runs did not include chemistry diagnostics for PAN so it is not possible at this time to directly compare the production of PAN at the emission regions associated with NO<sub>2</sub> and HNO<sub>3</sub>.

## Summary

We analyzed long range transport of NO<sub>2</sub> in order to investigate the performance of the MACC-II Reanalysis and WRF-Chem models compared to data from the GOME-2 satellite instrument. The GOME-2 data from Zien *et al.* [36] made it possible to look at a long range transport event of NO<sub>2</sub> using satellite retrieval.

Comparison of model and satellite data showed that the fronts associated with the cyclone lifted the NO<sub>2</sub> into the free troposphere. According to Jacob [24], the lifetime of the NO<sub>2</sub> would then be increased from hours in the boundary layer to days in the free troposphere allowing the NO<sub>2</sub> to be transported along with cyclone. The air mass factor used by Zien *et al.* [36] to compute the vertical column density assumed that all the NO<sub>2</sub> is homogeneously distributed in the clouds at a height of 3-5km. This leads to an underestimation of NO<sub>2</sub> below the clouds and at the emission sources. This underestimation is shown when comparing the satellite data to the model data. Both models show emissions from the UK and Europe that are not present in the GOME-2 data due to the low height of the plume in that region. However, the GOME-2 data by Zien *et al.* [36] was made for looking specifically at LRT events. The underestimation of NO<sub>2</sub> over emission regions for gome-2 data is due to the nature of the retrieval and is therefore expected.

The MACC-II Reanalysis model shows good spatial similarities to the GOME-2 data on September 30, and October 02, but poor spatial similarities on October 01. A large plume is seen originating from the UK in the model that is not detected in the satellite retrieval. This is in part due to the nature of the retrieval. The MACC-II Reanalysis model also shows higher background values over the ocean. This can be explained in part because the satellite values represent a tropospheric excess column calculated by

the satellite retrieval. The values in the plume represented in the model are much lower than that of the GOME-2 data. There could be several reasons for this including chemical conversion rates and boundary layer physics settings in the model. The plume is also wider than what is shown in the GOME-2 data. This is due to the coarser resolution of the MACC-II model.

The MACC-II and WRF-Chem 100km model simulations were then compared to each other. Both models show good spatial similarities between each other. The WRF-Chem run shows lower background values over the ocean and higher column values in the plume and over emission regions than the MACC-II Reanalysis and therefore better agrees with the GOME-2 data values. In general, differences between models can be explained due to differences in chemistry, and representation of physical processes in the atmosphere. The WRF-Chem model is an online model so chemistry and meteorology are able to interact and change depending on changing conditions. The MACC-II Reanalysis model is coupled and the chemistry cannot effect meteorological conditions. The chemistry and emission inventories are also different between the models.

The 50km resolution run of the WRF-Chem model better agrees with the GOME-2 data both spatially and regarding the magnitude of the VCD than the MACC-II Reanalysis. More  $\text{NO}_2$  is transported in the cyclone in the high resolution run as compared to the MACC-II, but emission regions are still seen in the model as is expected.

Looking at the chemistry and weather diagnostic fields in the WRF-Chem model, we were able to see that most of the  $\text{NO}_2$  was converted into  $\text{HNO}_3$  before it was able to exit the boundary layer. This leads to less  $\text{NO}_2$  being transported in the cyclone and is a reasonable explanation why the GOME-2 values inside the plume over the ocean away from emission areas, were

higher than that of the WRF-Chem.

The  $\text{HNO}_3$  acts as a sink for  $\text{NO}_2$  through the reaction between  $\text{NO}_2$  and  $\text{OH}$ , and is also effected by wet scavenging. The model shows that almost all of the  $\text{HNO}_3$  converted from  $\text{NO}_2$  is scavenged out during the transport process.

PAN is the other trace gas looked at. Since most of the  $\text{NO}_2$  is transformed into  $\text{HNO}_3$  in the model, The amount of PAN produced through chemical conversion at the emission region is small. It would be helpful to look at chemical diagnostic fields for PAN as well, to specify the conversion rates in more detail.

$\text{NO}_2$  long range transport events can transport air pollution from emission regions to pristine regions. Both models are able to spatially represent the LRT in the cyclone. However, they do not show as high  $\text{NO}_2$  VCDs inside the plume as compared to the satellite. This is most likely due to the high conversion rates of  $\text{NO}_2$  to  $\text{HNO}_3$ , but could also be attributed to boundary layer physics settings, or an underestimation of trace gas emissions in the emission inventories used.



In order to better identify reasons why the WRF-Chem and satellite retrieval values differ inside the plume, several more runs of the model will need to be completed. Changing the chemistry settings inside the model may slow the conversion of the  $\text{NO}_2$  and allow it to be transported out of the boundary layer. Combining this with changes in boundary layer physics and emissions could lead to better agreement with the satellite data.

We would also like to run the model at higher resolutions. We saw that with increased resolution came increased agreement between the model and satellite. If the resolution is increased further, the agreement may increase as well.

Looking at other diagnostic fields such as advection of the trace gasses output by the WRF-Chem model may be beneficial in order to better understand why the  $\text{NO}_2$  is not being transported as far.

We would also like to look at chemistry diagnostic fields of the MACC-II model in order to understand why background values are higher and plume values are lower, but these are not included in the standard product.

It would also be useful to look at other LRT cases. This study focused on one specific case of LRT. Comparing the results of this study to that of other LRT events could help to verify that the models are representing the transport properly and to see if the values in the plumes are still underestimated in the model data when compared to the satellite retrievals.



# Bibliography

1. Antonakaki, T., Arola, A., Benedictow, A., *et al.* Validation report of the MACC near real time global atmospheric composition service System evolution and performance statistics (2013).
2. Aschmann, J., Sinnhuber, B. M., Atlas, E. L. & Schauffler, S. M. Modeling the transport of very short-lived substances into the tropical upper troposphere and lower stratosphere. *Atmospheric Chemistry and Physics Discussions* **9**, 18511–18543 (2009).
3. AVHRR. *Dundee Satellite Receiving Station*. web. <http://www.sat.dundee.ac.uk>. 2010.
4. Barth, M. C., Kim, S. W., Wang, C., *et al.* Cloud-scale model intercomparison of chemical constituent transport in deep convection. *Atmospheric Chemistry and Physics Discussions* **7**, 8035–8085 (2007).
5. Beirle, S., Huntrieser, H. & Wagner, T. Direct satellite observation of lightning-produced NO<sub>x</sub>. *Atmospheric Chemistry and Physics* **10**, 10965–10986 (2010).
6. Beirle, S., Boersma, K. F., Platt, U., Lawrence, M. G. & Wagner, T. Megacity Emissions and Lifetimes of Nitrogen Oxides Probed from Space. *Science* **333**, 1737–1739 (2011).
7. Beirle, S., Platt, U., Wenig, M. & Wagner, T. NO<sub>x</sub> production by lightning estimated with GOME. *Advances in Space Research* **34**, 793–797 (2004).
8. Boersma, K. F. Error analysis for tropospheric NO<sub>2</sub> retrieval from space. *Journal of Geophysical Research* **109** (2004).
9. Bovensmann, H., Burrows, J. P., Buchwitz, M., *et al.* SCIAMACHY: Mission Objectives and Measurement Modes. *Journal of the Atmospheric Sciences* **56**, 127–150 (1999).
10. Burrows, J. P., Buchwitz, M., Rozanov, V., *et al.* The Global Ozone Monitoring Experiment (GOME): Mission, instrument concept, and first scientific results. *European Space Agency, (Special Publication) ESA SP 1*, 585–590 (1997).
11. Burrows, J. P., Platt, U., Borrell, P., Borrell, U. & Peter, P. *BOOK: The remote sensing of tropospheric composition from space* **February**, 549 (2011).

12. Callies, J., Corpaccioli, E., Eisinger, M., Hahne, A. & Lefebvre, A. GOME-2 - Metop's second-generation sensor for operational ozone monitoring. *ESA Bulletin-European Space Agency* **102**, 28–36 (2000).
13. Christoudias, T., Pozzer, A. & Lelieveld, J. Influence of the North Atlantic Oscillation on air pollution transport. *Atmospheric Chemistry and Physics* **12**, 869–877 (2012).
14. Crawford, J. Clouds and trace gas distributions during TRACE-P. *Journal of Geophysical Research* **108** (2003).
15. Ding, A., Wang, T., Xue, L., *et al.* Transport of north China air pollution by midlatitude cyclones: Case study of aircraft measurements in summer 2007. *Journal of Geophysical Research: Atmospheres* **114**, 1–16 (2009).
16. Ehhalt, D. H., Rohner, F. & Wahner, A. Sources and Distribution of NO<sub>x</sub> in the Upper Troposphere at northern mid-latitudes. *Journal of Geophysical Research* **97** (1992).
17. EPA. Nitrogen dioxide health effects web. <http://www.epa.gov>. Aug. 2014.
18. Grell, G. A., Peckham, S. E., Schmitz, R., *et al.* Fully coupled chemistry within the WRF model. *Atmospheric Environment* **39**, 6957–6975 (2005).
19. Hawcroft, M. K., Stringer, M. A., Hodges, K. I., Dacre, H. F. & Gate, E. an Extratropical Cyclone Database. *American Meteorological Society*, 1–10 (2010).
20. Horstmeyer, S. The Norwegian Cyclone Model (2015).
21. Houze, R. A. & Hobbs, P. V. Organization and structure of precipitating cloud systems. *Deep Sea Research Part B. Oceanographic Literature Review* **30**, 442 (1983).
22. Houze, R. A. & Hobbs, P. V. Organization and structure of precipitating cloud systems. *Deep Sea Research Part B. Oceanographic Literature Review* **30**, 442 (1983).
23. Inness, A., Baier, F., Benedetti, A., *et al.* The MACC reanalysis: An 8 yr data set of atmospheric composition. *Atmospheric Chemistry and Physics* **13**, 4073–4109 (2013).
24. Jacob, D. Oxidation Power of the Troposphere. *Introduction to Atmospheric Chemistry*. **3**, 199–219 (1999).
25. Klich, C. A. & Fuelberg, H. E. The role of horizontal model resolution in assessing the transport of CO in a middle latitude cyclone using WRF-Chem. *Atmospheric Chemistry and Physics* **14**, 609–627 (2014).
26. Kokhanovsky, A. A. & Rozanov, V. V. Retrieval of NO<sub>2</sub> vertical columns under cloudy conditions: A sensitivity study based on SCIATRAN calculations. *Atmospheric Research* **93**, 695–699 (2009).

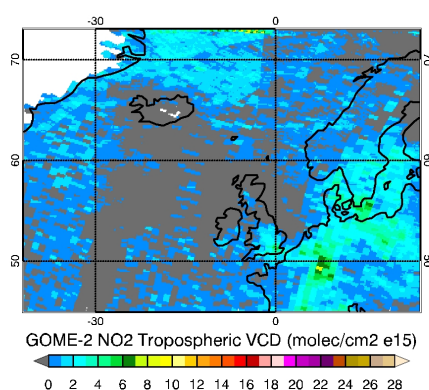
27. Lin, M., Holloway, T., Carmichael, G. R. & Fiore, A. M. Quantifying pollution inflow and outflow over East Asia in spring with regional and global models. *Atmospheric Chemistry and Physics* **10**, 4221–4239 (2010).
28. MACC-II. *MACC Project - Project Description*. "MACC Project - Project Description" web. <https://www.gmes-atmosphere.eu/about/project/>. 2015.
29. OECD. *OECD Glossary of Statistical Terms - Long-range Transport of Air Pollutants Definition*. "OECD Glossary of Statistical Terms - Long-range Transport of Air Pollutants Definition" web. <http://stats.oecd.org/glossary/detail.asp?ID=1558>. 2015.
30. Rastigejev, Y., Park, R., Brenner, M. P. & Jacob, D. J. Resolving intercontinental pollution plumes in global models of atmospheric transport. *Journal of Geophysical Research: Atmospheres* **115** (2010).
31. Richter, A. & Burrows, J. P. Tropospheric NO<sub>2</sub> from GOME measurements. *Adv. Space Res* **2**, 1–11 (2001).
32. Schaub, D., Weiss, A. K., Kaiser, J. W., *et al.* A transboundary transport episode of nitrogen dioxide as observed from GOME and its impact in the Alpine region. *Atmospheric Chemistry and Physics Discussions* **4**, 5103–5134 (2004).
33. Stohl, A., Huntrieser, H., Richter, A., *et al.* Rapid intercontinental air pollution transport associated with a meteorological bomb. *Atmospheric Chemistry and Physics Discussions* **3**, 2101–2141 (2003).
34. Velders, G. J. M., Granier, C., Portmann, R. W., *et al.* column distributions: Comparing three-dimensional model calculations with GOME measurements. *Journal of Geophysical Research* **106**, 12643 (2001).
35. Wenig, M., Spichtinger, N., Stohl, A., *et al.* Intercontinental transport of nitrogen oxide pollution plumes. *Atmospheric Chemistry and Physics Discussions* **2**, 2151–2165 (2002).
36. Zien, A. W., Richter, A., Hilboll, A., Blechschmidt, A. M. & Burrows, J. P. Systematic analysis of tropospheric NO<sub>2</sub> long-range transport events detected in GOME-2 satellite data. *Atmospheric Chemistry and Physics* **14**, 7367–7396 (2014).



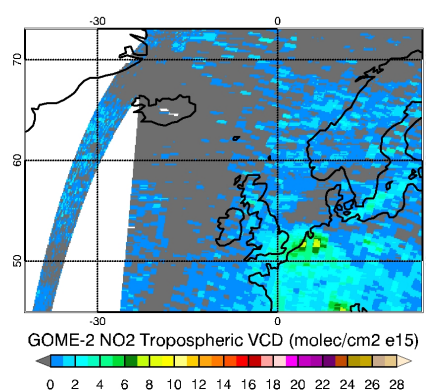
# Appendices

## A.1 GOME-2

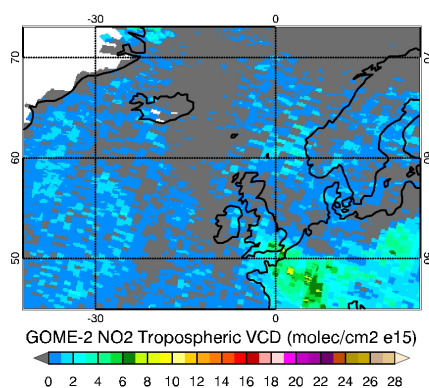
Complete time series for GOME-2 NO<sub>2</sub> satellite retrieval from September 25, 2010 to October 10, 2010. The satellite data shows the progression of the LRT event in the cyclone from formation to dispersion.



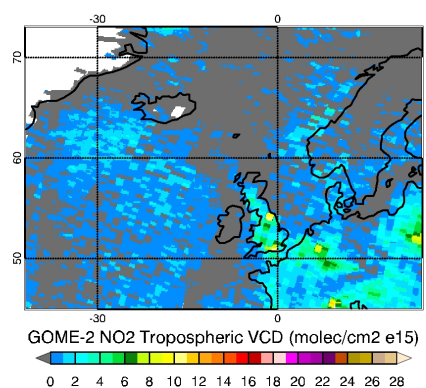
(a) September 25, 2010



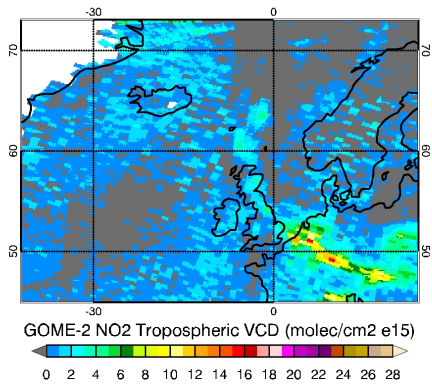
(b) September 26, 2010



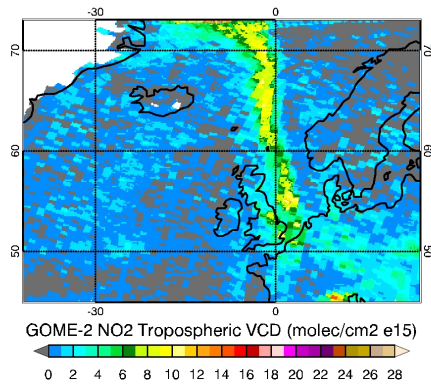
(a) September 27, 2010



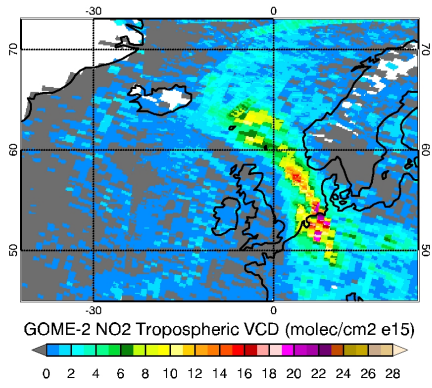
(b) September 28, 2010



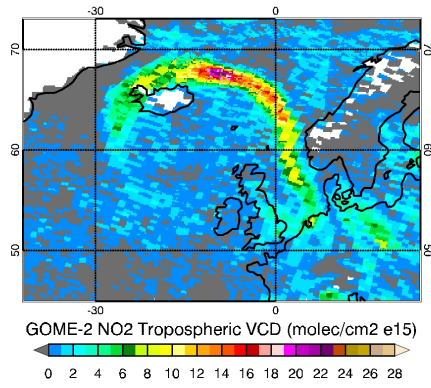
(a) September 29, 2010



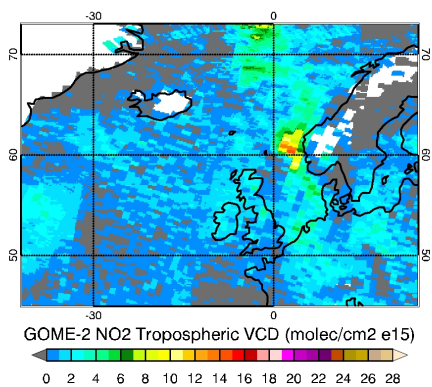
(b) September 30, 2010



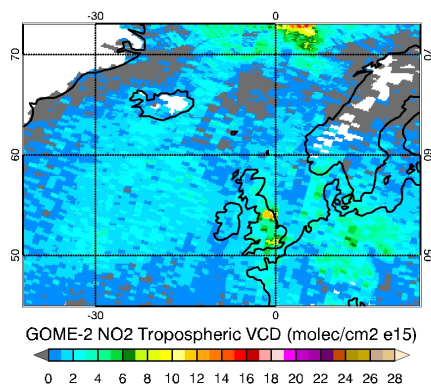
(a) October 01, 2010



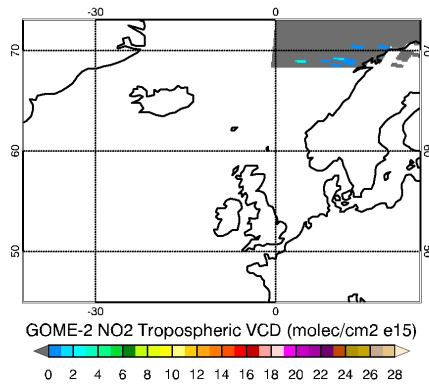
(b) October 02, 2010



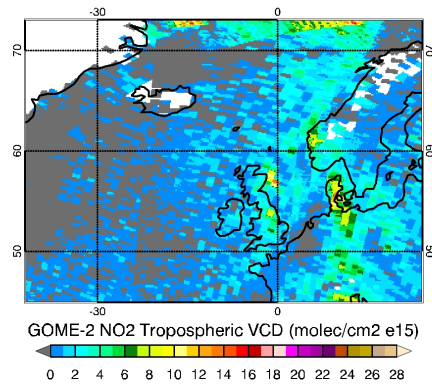
(a) October 03, 2010



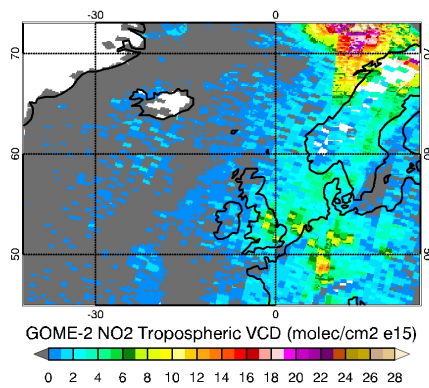
(b) October 04, 2010



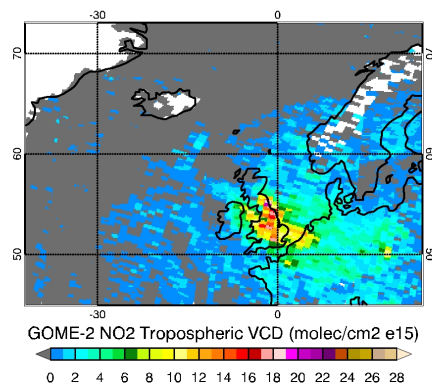
(a) October 05, 2010



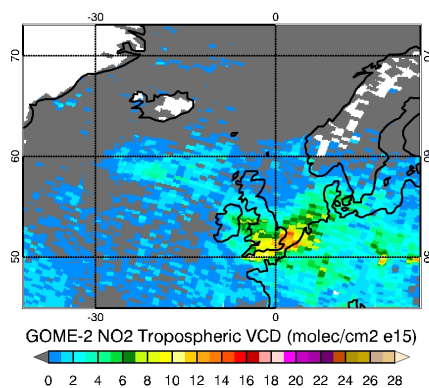
(b) October 06, 2010



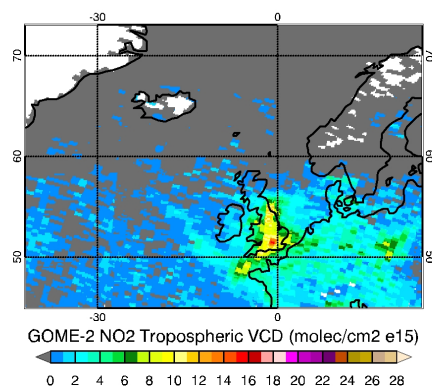
(a) October 07, 2010



(b) October 08, 2010



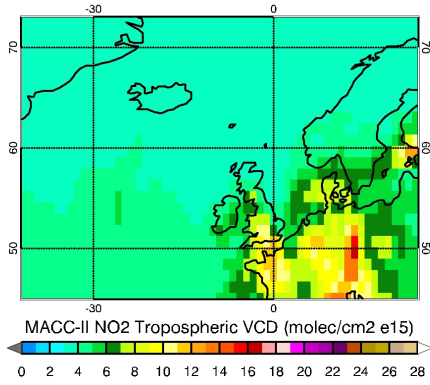
(a) October 09, 2010



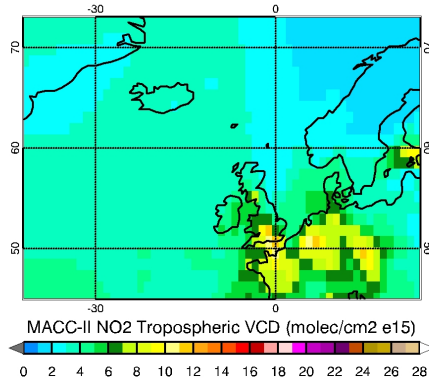
(b) October 10, 2010

## A.2 MACC-II Reanalysis

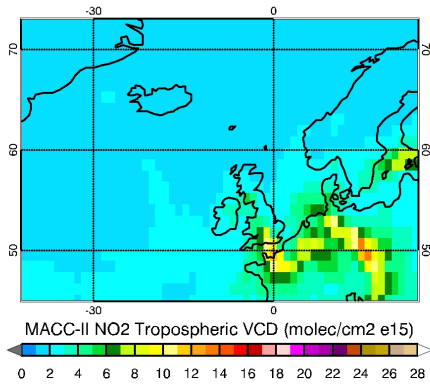
Complete time series for MACC-II Reanalysis NO<sub>2</sub> LRT. Series spans from September 26, 2010 and extends through October 08, 2010 with an output time step of 6 hours.



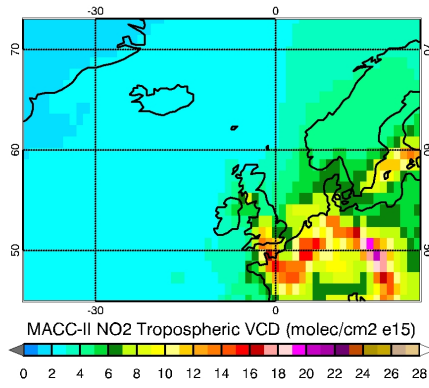
(a) September 26, 2010 Time step 0



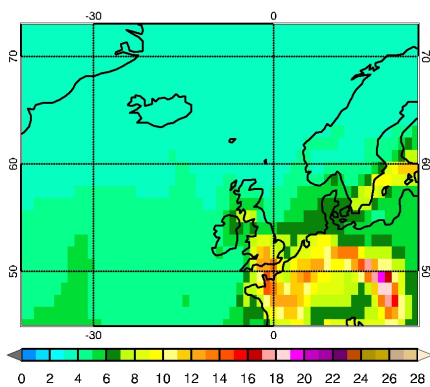
(b) September 26, 2010 Time step 1



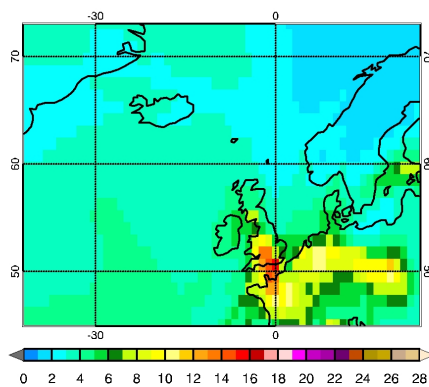
(a) September 26, 2010 Time step 2



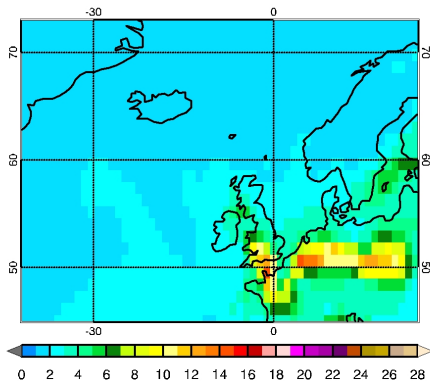
(b) September 26, 2010 Time step 3



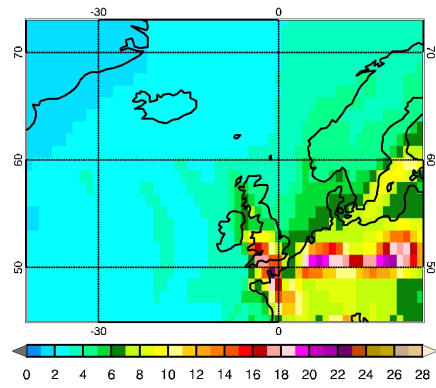
(a) September 27, 2010 Time step 0



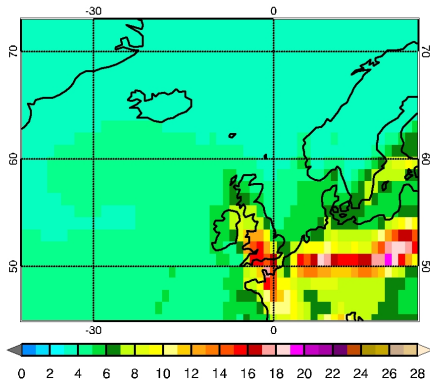
(b) September 27, 2010 Time step 1



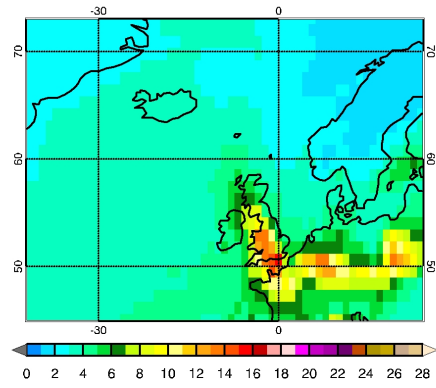
(a) September 27, 2010 Time step 2



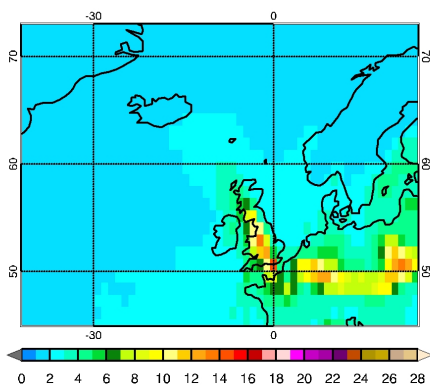
(b) September 27, 2010 Time step 3



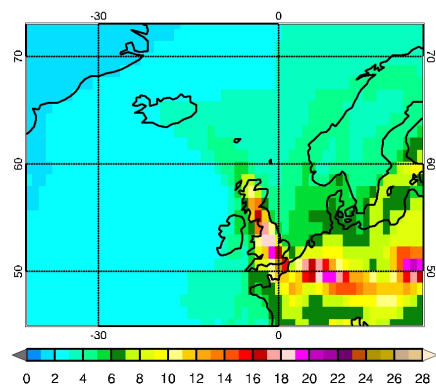
(a) September 28, 2010 Time step 0



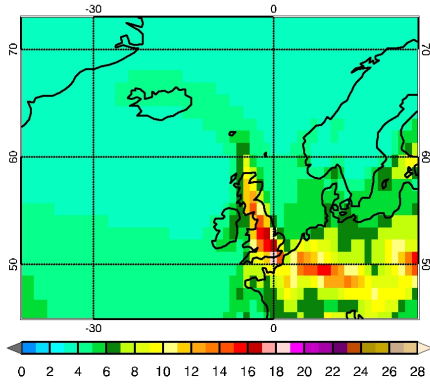
(b) September 28, 2010 Time step 1



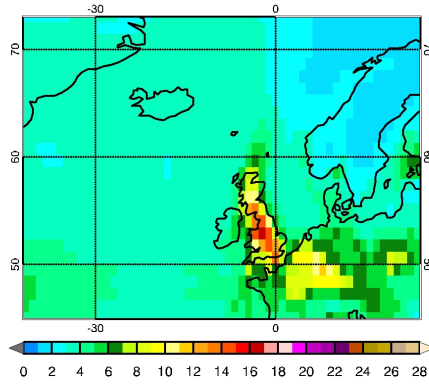
(a) September 28, 2010 Time step 2



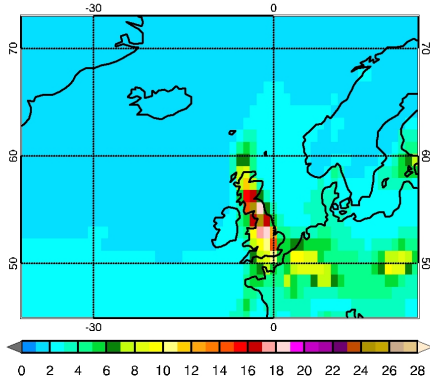
(b) September 28, 2010 Time step 3



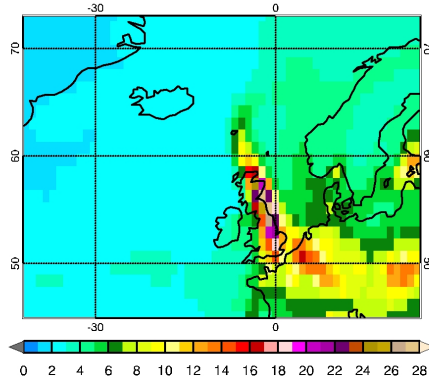
(a) September 29, 2010 Time step 0



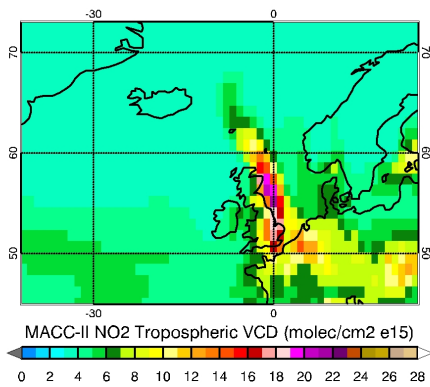
(b) September 29, 2010 Time step 1



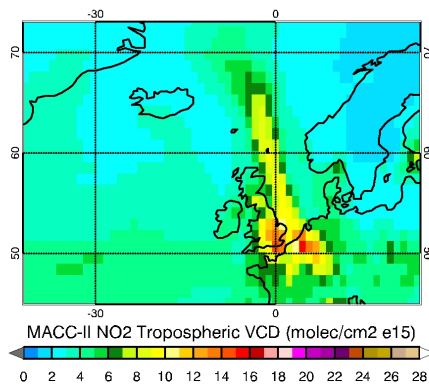
(a) September 29, 2010 Time step 2



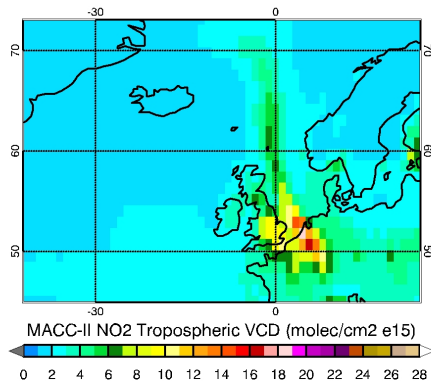
(b) September 29, 2010 Time step 3



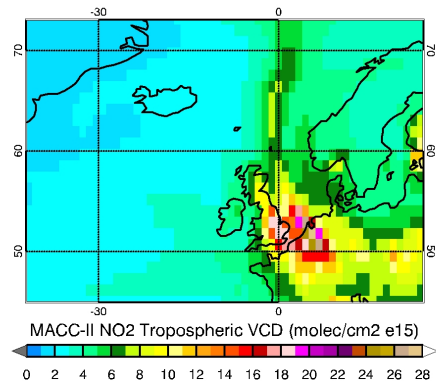
(a) September 30, 2010 Time step 0



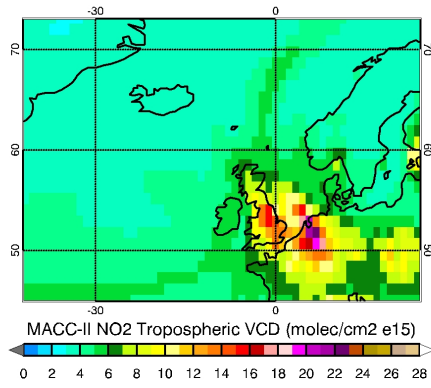
(b) September 30, 2010 Time step 1



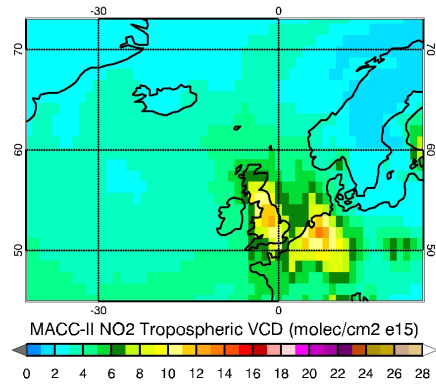
(a) September 30, 2010 Time step 2



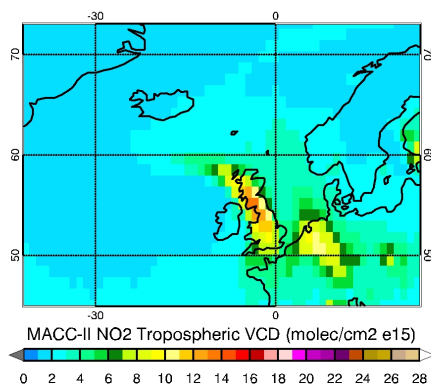
(b) September 30, 2010 Time step 3



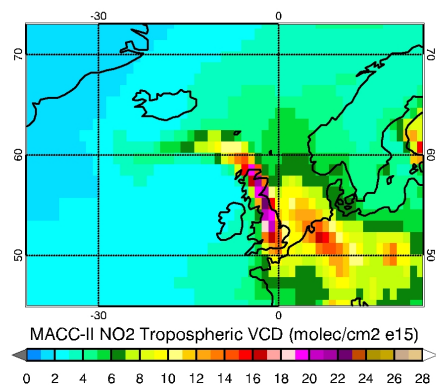
(a) October 01, 2010 Time step 0



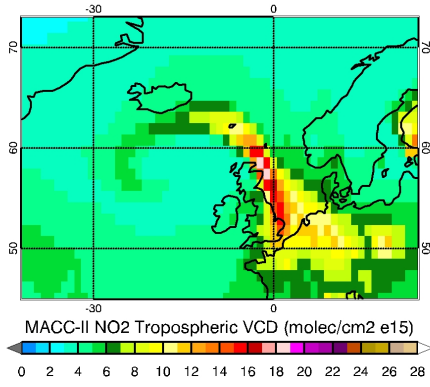
(b) October 01, 2010 Time step 1



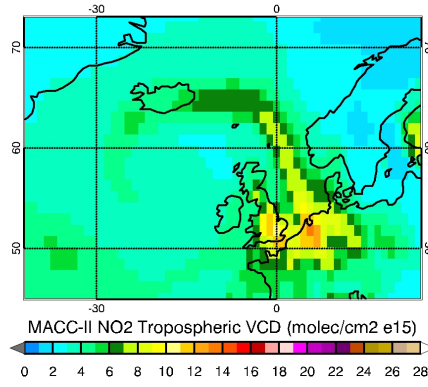
(a) October 01, 2010 Time step 2



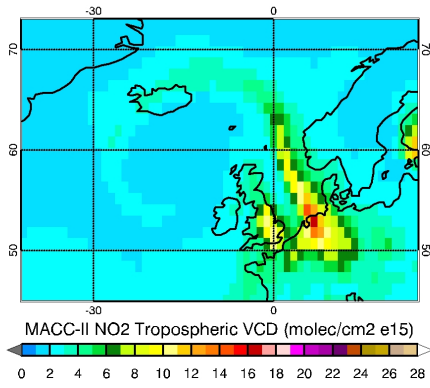
(b) October 01, 2010 Time step 3



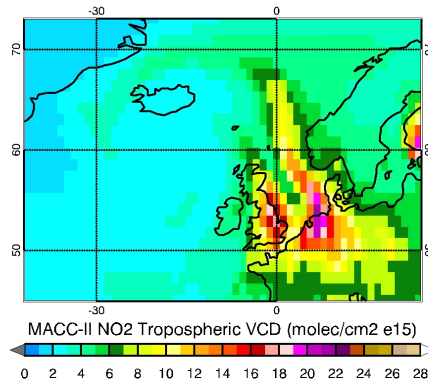
(a) October 02, 2010 Time step 0



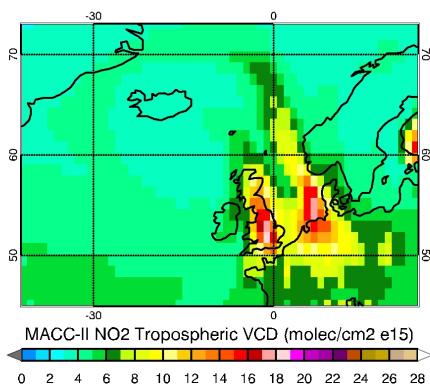
(b) October 02, 2010 Time step 1



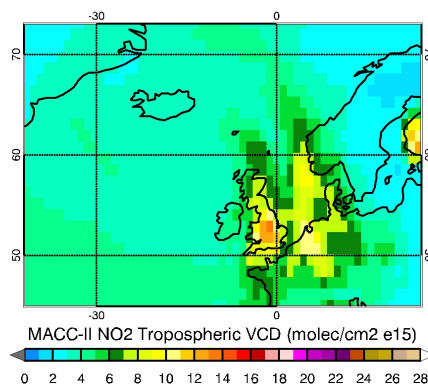
(a) October 02, 2010 Time step 2



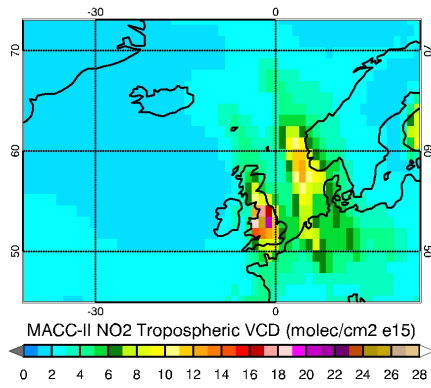
(b) October 02, 2010 Time step 3



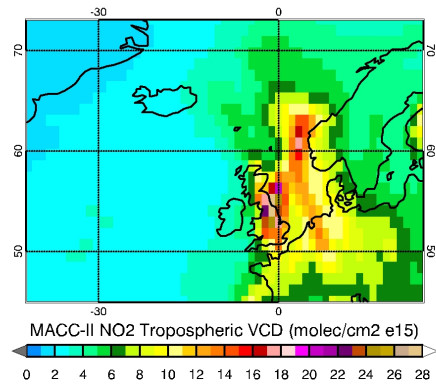
(a) October 03, 2010 Time step 0



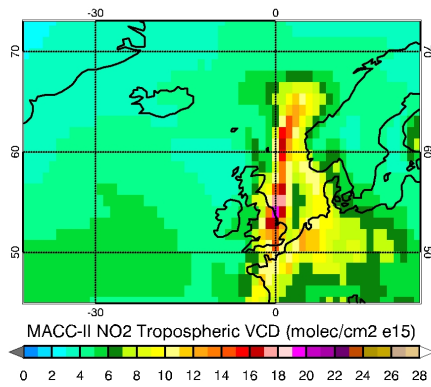
(b) October 03, 2010 Time step 1



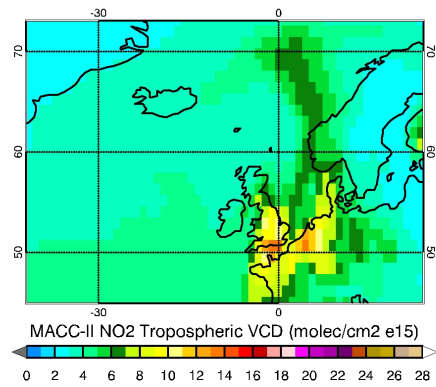
(a) October 03, 2010 Time step 2



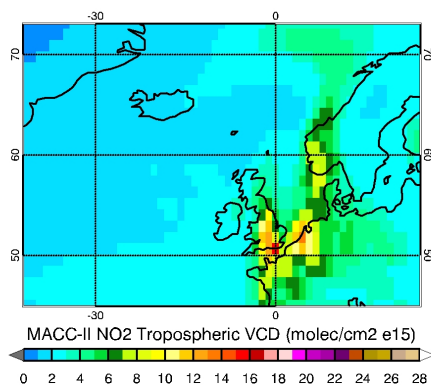
(b) October 03, 2010 Time step 3



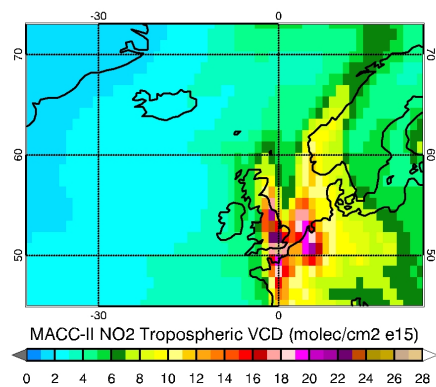
(a) October 04, 2010 Time step 0



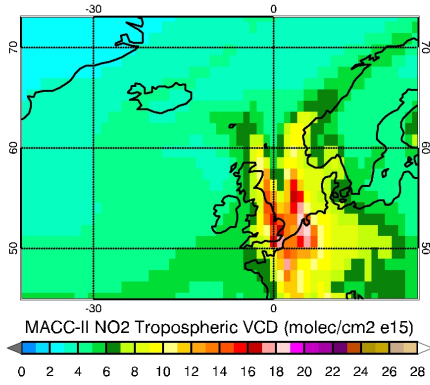
(b) October 04, 2010 Time step 1



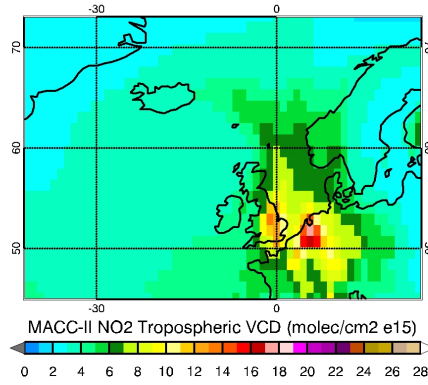
(a) October 04, 2010 Time step 2



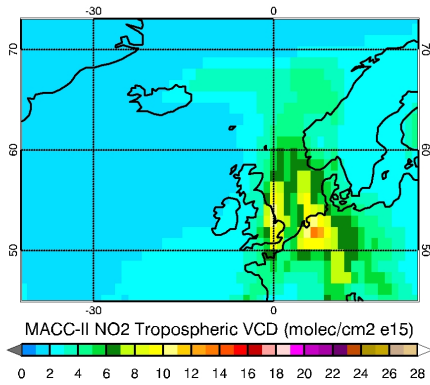
(b) October 04, 2010 Time step 3



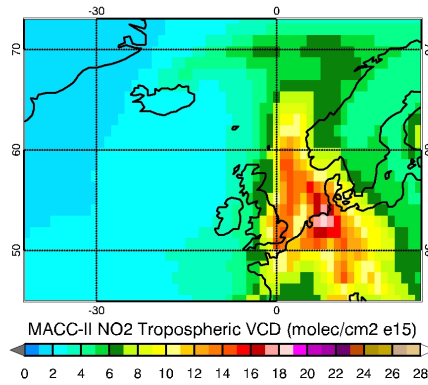
(a) October 05, 2010 Time step 0



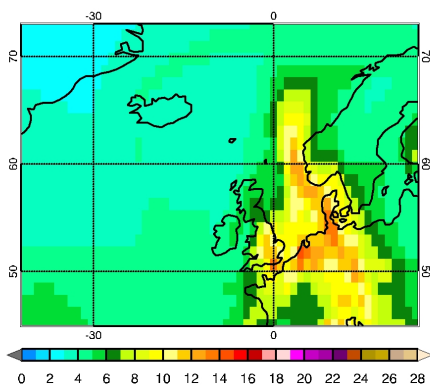
(b) October 05, 2010 Time step 1



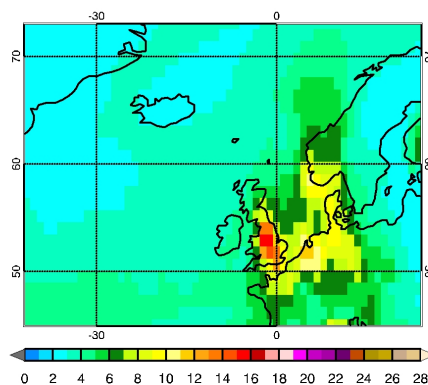
(a) October 05, 2010 Time step 2



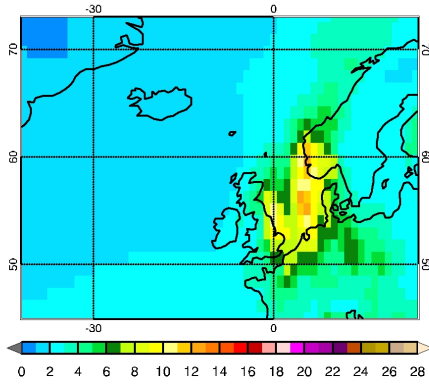
(b) October 05, 2010 Time step 3



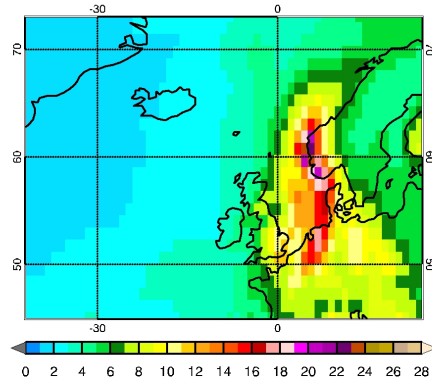
(a) October 06, 2010 Time step 0



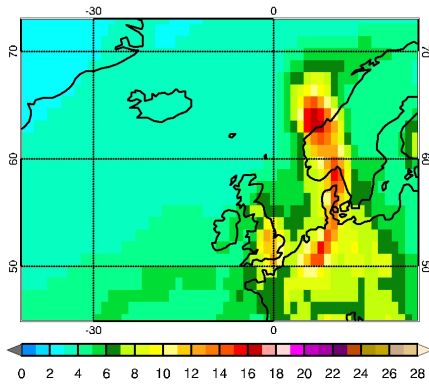
(b) October 06, 2010 Time step 1



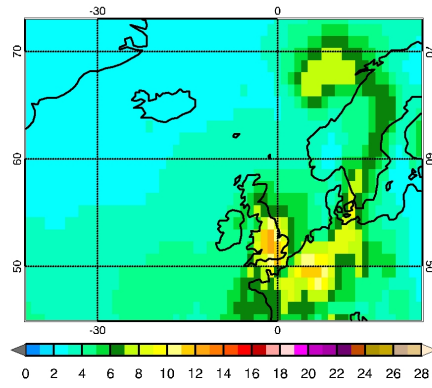
(a) October 06, 2010 Time step 2



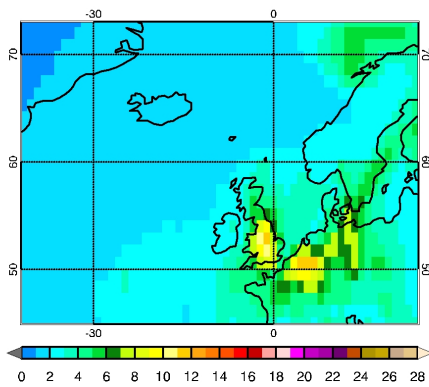
(b) October 06, 2010 Time step 3



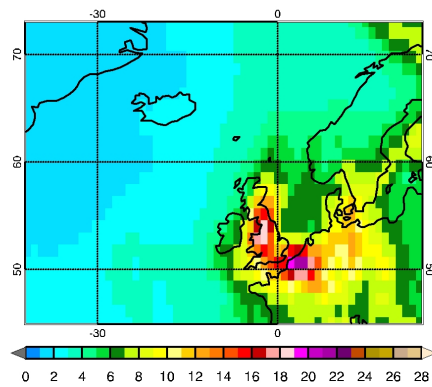
(a) October 07, 2010 Time step 0



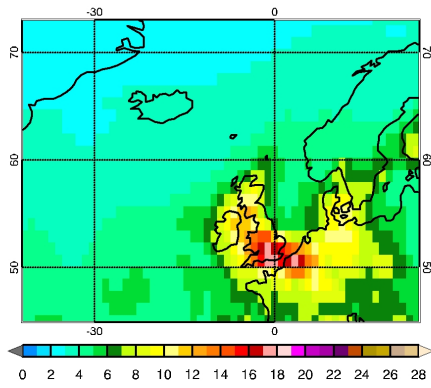
(b) October 07, 2010 Time step 1



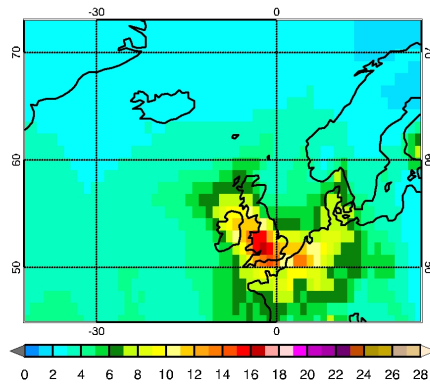
(a) October 07, 2010 Time step 2



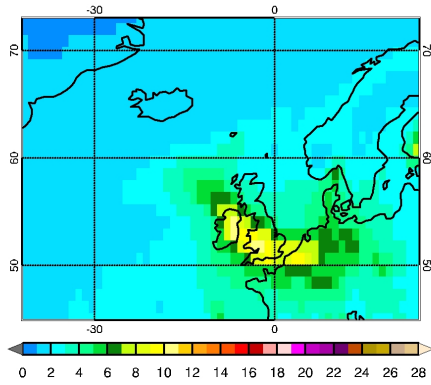
(b) October 07, 2010 Time step 3



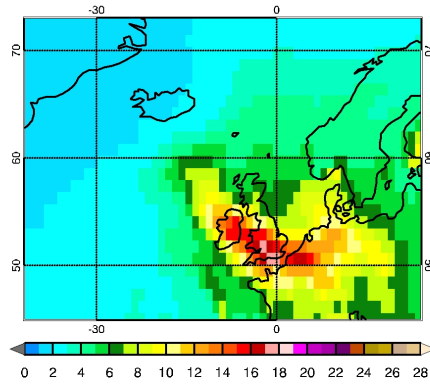
(a) October 08, 2010 Time step 0



(b) October 08, 2010 Time step 1



(a) October 08, 2010 Time step 2

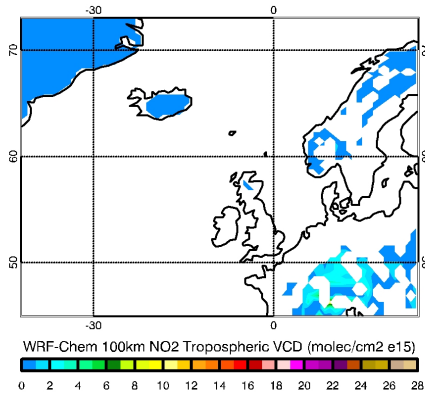


(b) October 08, 2010 Time step 3

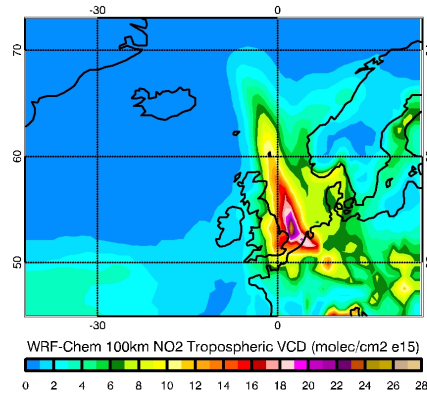
## A.3 WRF-Chem

The WRF-Chem model was run at 2 different resolutions, 100km and 50km, in order to see if increased resolution lead to better agreement with the satellite data. The runs cover the dates between September 30, 2010 and October 04, 2010, and have an output time step of 3 hours.

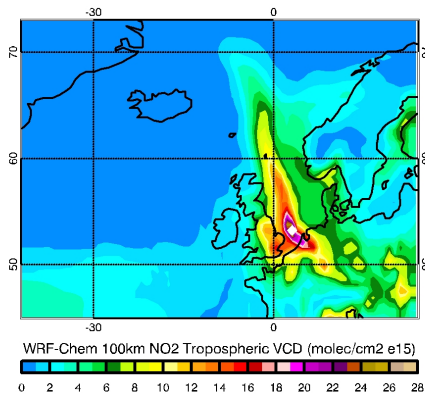
### A.3.1 100km resolution NO<sub>2</sub>



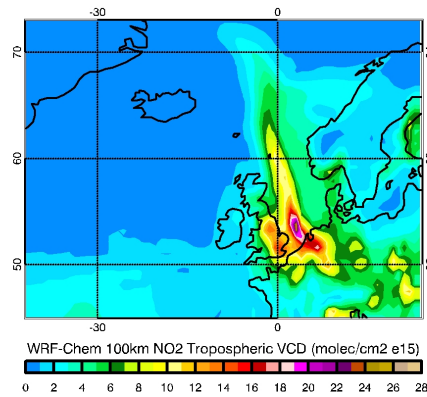
(a) September 30, 2010 Time step 0



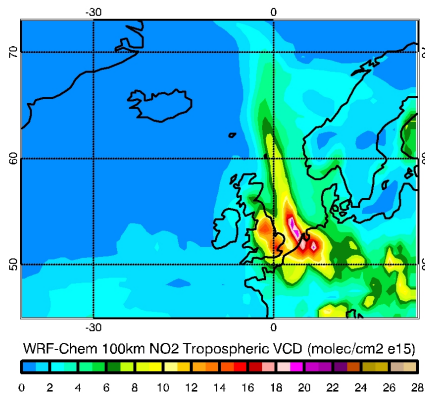
(b) September 30, 2010 Time step 1



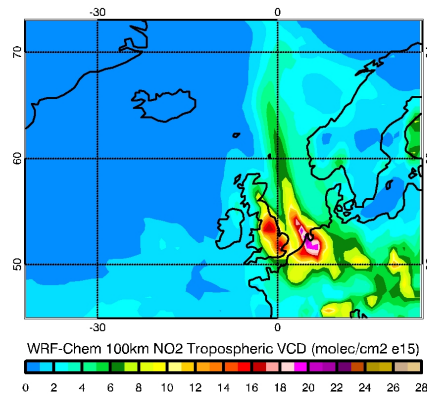
(a) September 30, 2010 Time step 2



(b) September 30, 2010 Time step 3



(a) September 30, 2010 Time step 4



(b) September 30, 2010 Time step 5

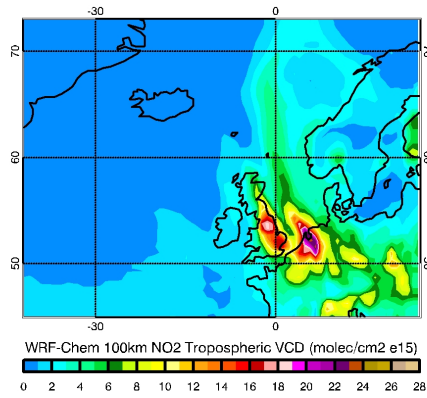
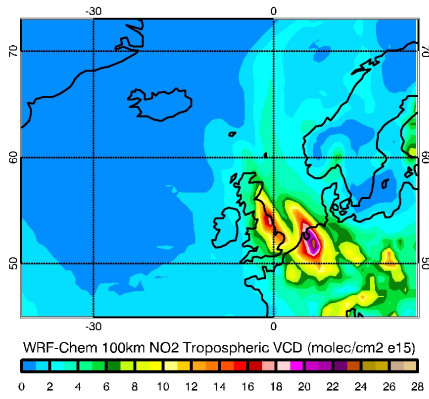
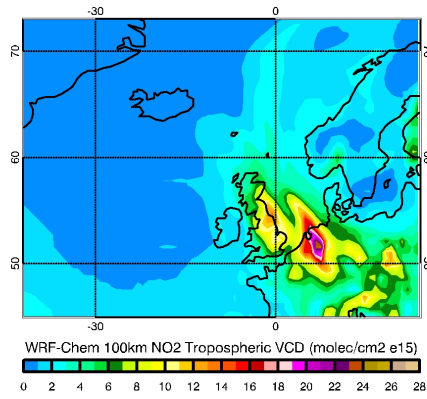


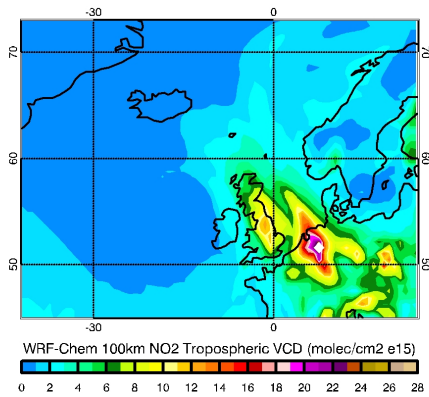
**Fig. A.38.:** September 30, 2010 Time step 6



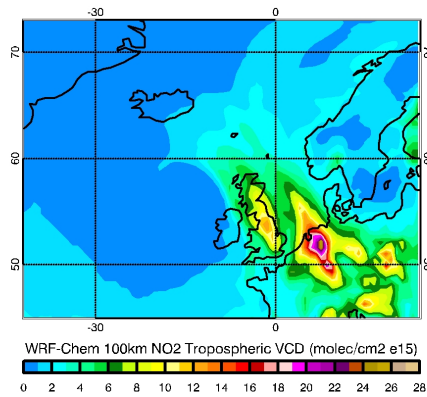
**(a)**October 01, 2010 Time step 0



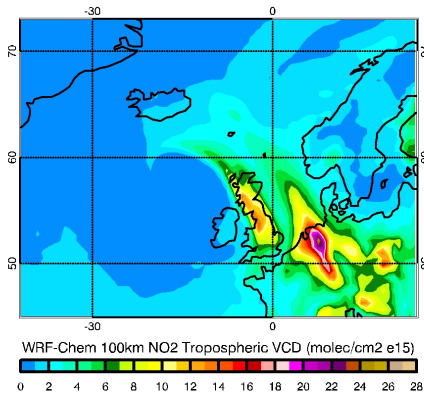
**(b)**October 01, 2010 Time step 1



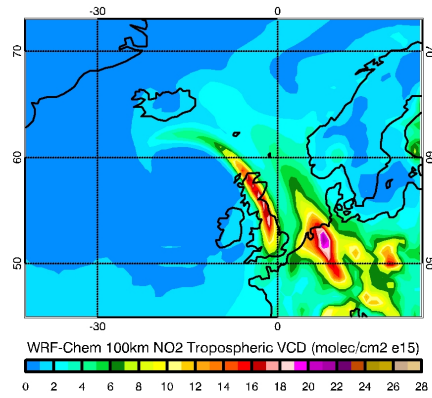
**(a)**October 01, 2010 Time step 2



**(b)**October 01, 2010 Time step 3



(a) October 01, 2010 Time step 4



(b) October 01, 2010 Time step 5

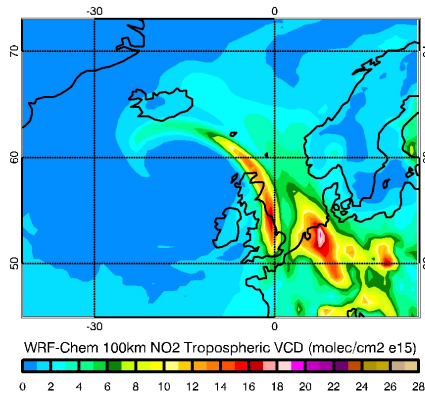
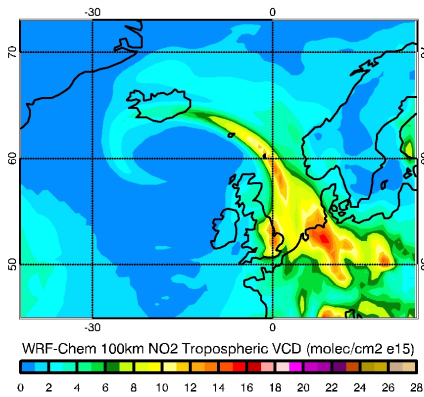
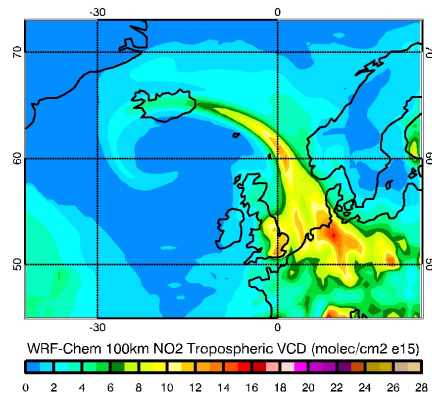


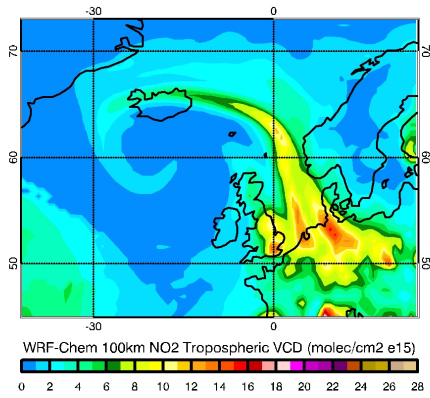
Fig. A.42.: October 01, 2010 Time step 6



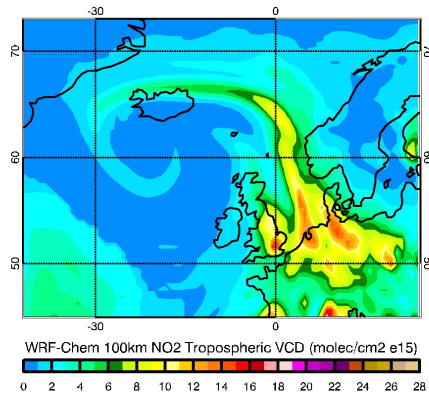
(a) October 02, 2010 Time step 0



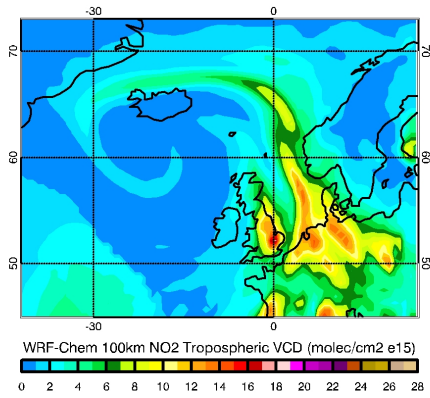
(b) October 02, 2010 Time step 1



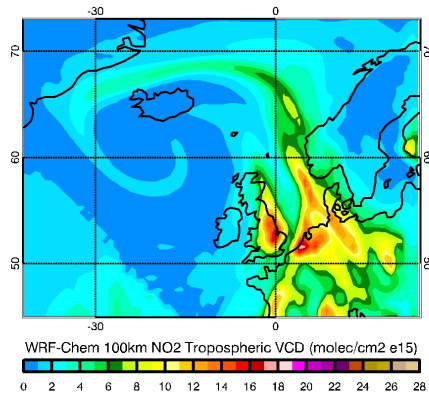
(a) October 02, 2010 Time step 2



(b) October 02, 2010 Time step 3



(a) October 02, 2010 Time step 4



(b) October 02, 2010 Time step 5

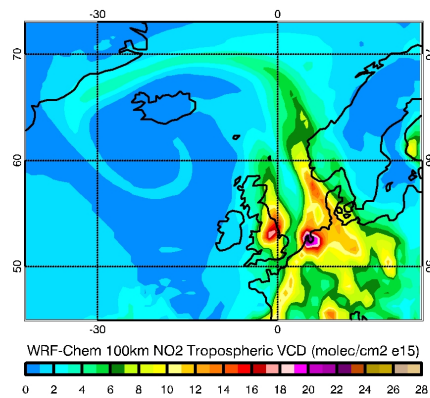
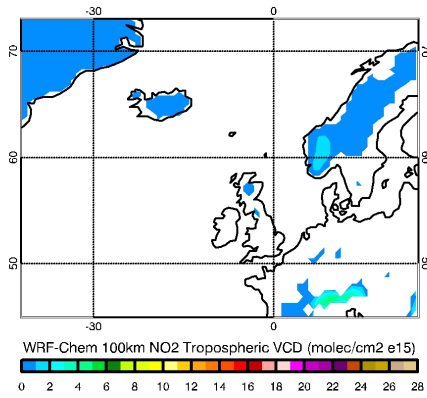
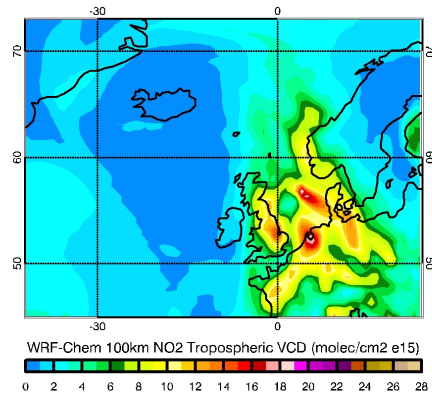


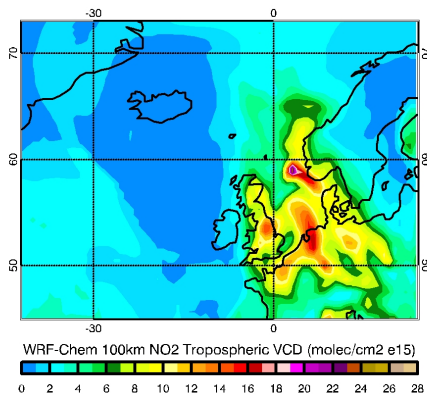
Fig. A.46.: October 02, 2010 Time step 6



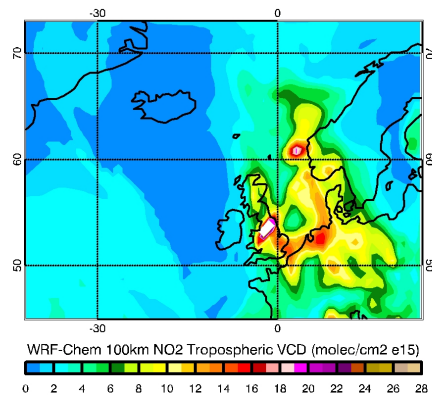
(a) October 03, 2010 Time step 0



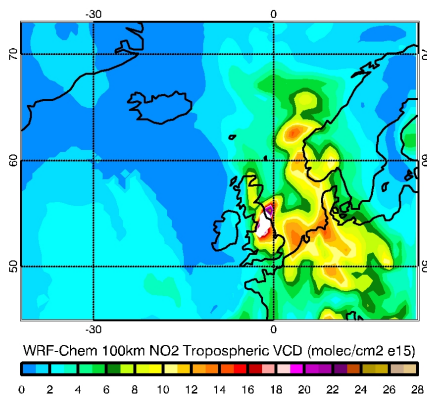
(b) October 03, 2010 Time step 1



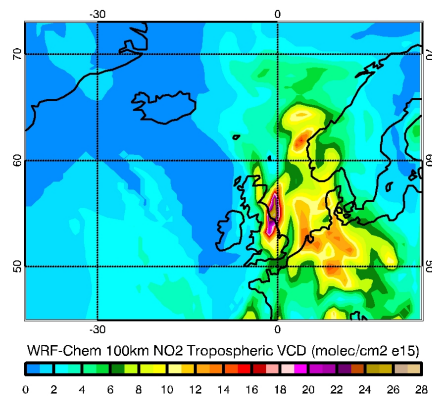
(a) October 03, 2010 Time step 2



(b) October 03, 2010 Time step 3



(a) October 03, 2010 Time step 4



(b) October 03, 2010 Time step 5

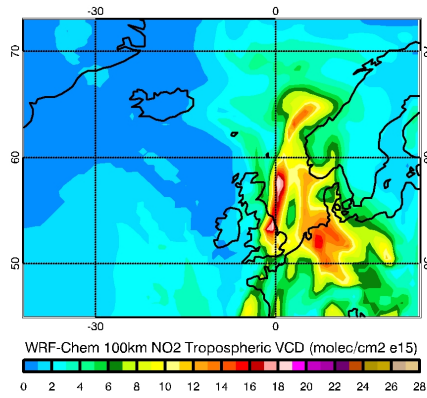
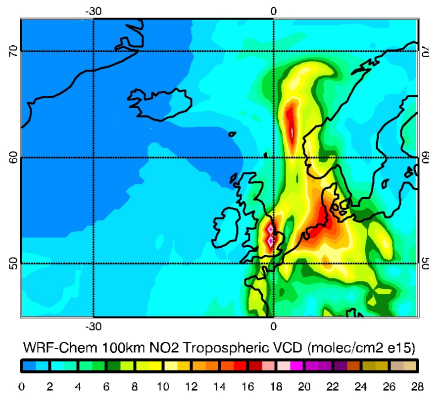
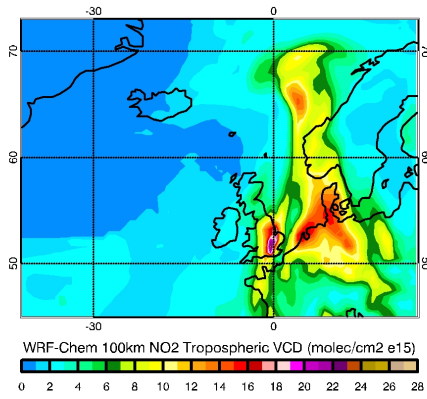


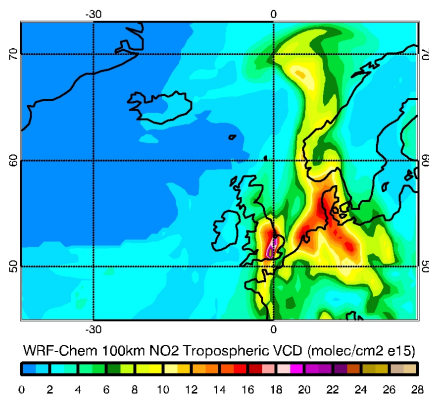
**Fig. A.50.:** October 03, 2010 Time step 6



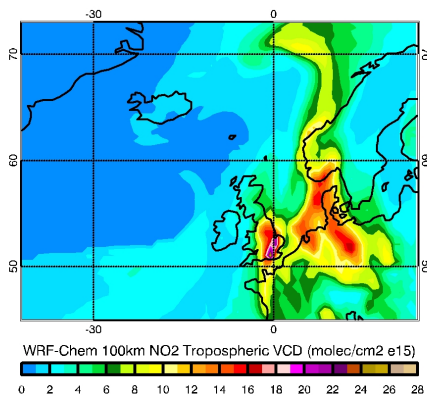
**(a)**October 04, 2010 Time step 0



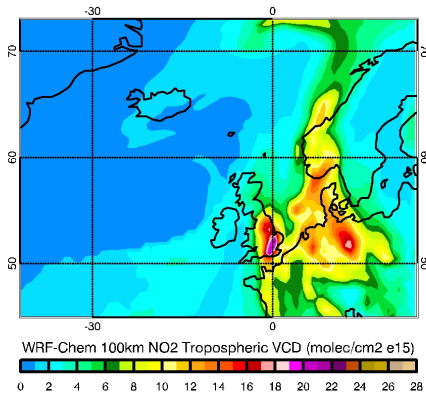
**(b)**October 04, 2010 Time step 1



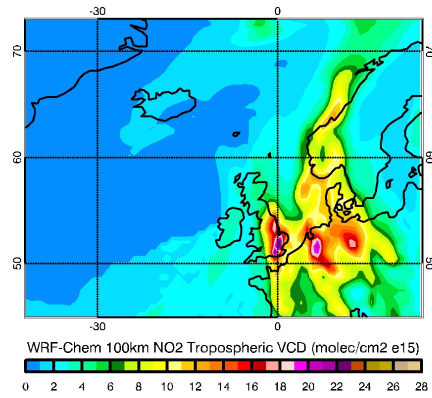
**(a)**October 04, 2010 Time step 2



**(b)**October 04, 2010 Time step 3



(a) October 04, 2010 Time step 4



(b) October 04, 2010 Time step 5

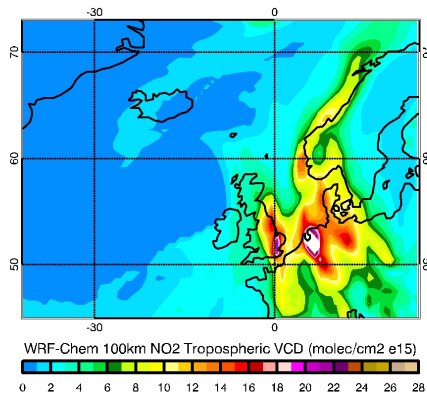
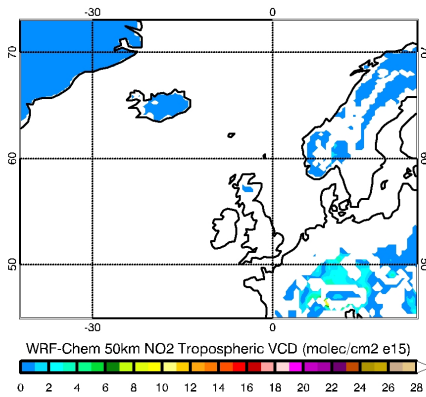
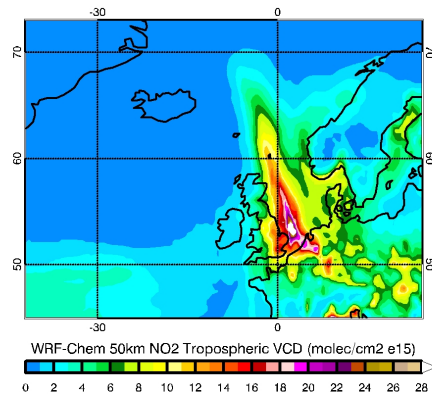


Fig. A.54.: October 04, 2010 Time step 6

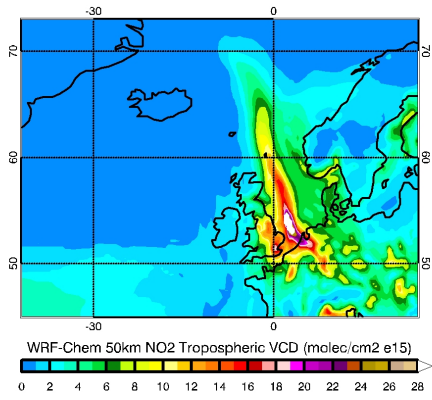
### A.3.2 50km resolution NO<sub>2</sub>



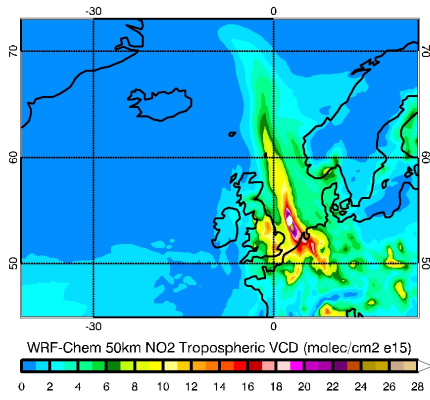
(a) September 30, 2010 Time step 0



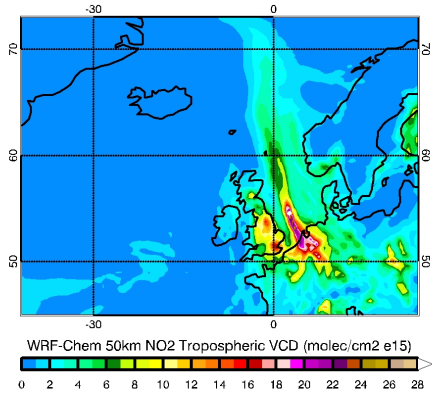
(b) September 30, 2010 Time step 1



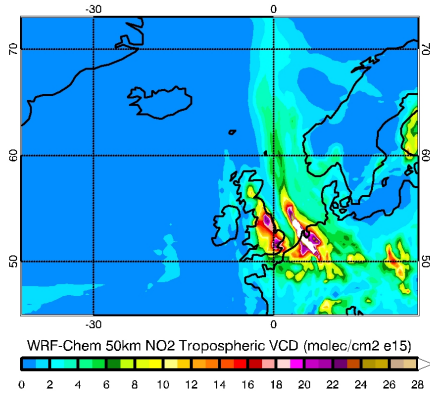
(a) September 30, 2010 Time step 2



(b) September 30, 2010 Time step 3



(a) September 30, 2010 Time step 4



(b) September 30, 2010 Time step 5

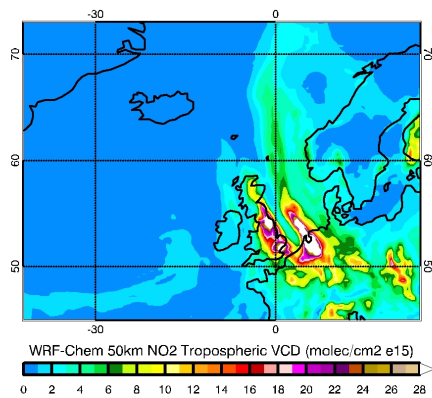
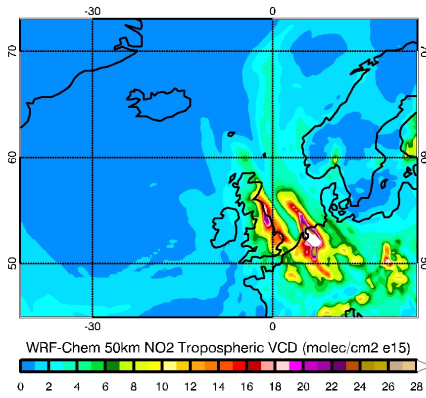
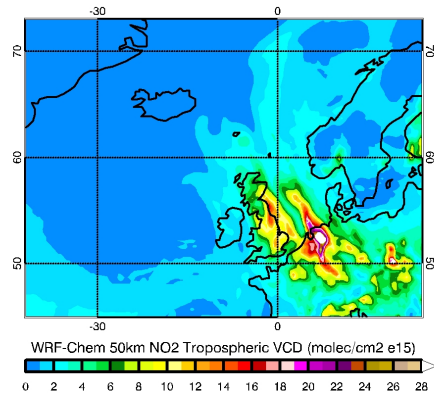


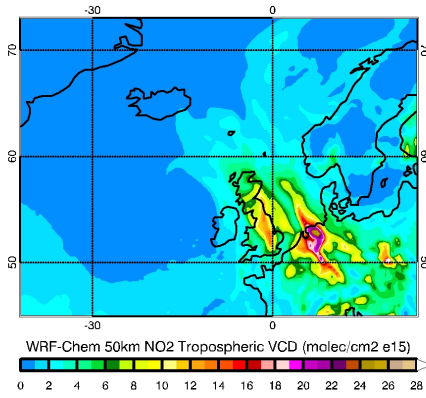
Fig. A.58.: September 30, 2010 Time step 6



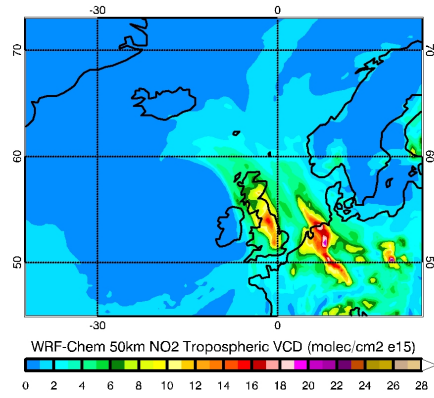
(a) October 01, 2010 Time step 0



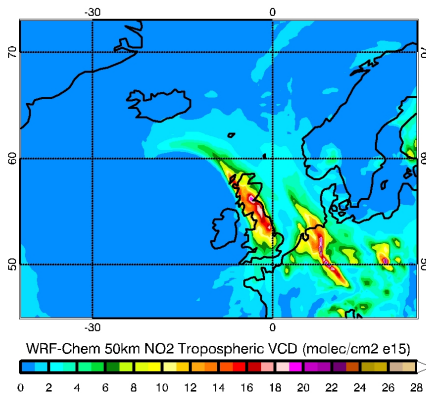
(b) October 01, 2010 Time step 1



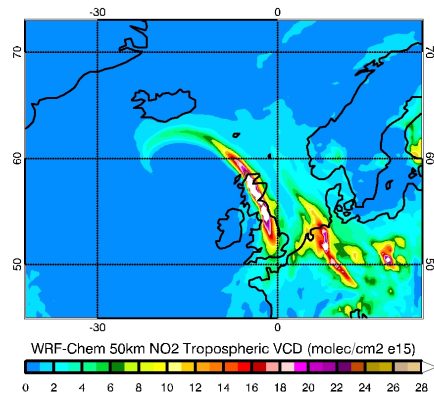
(a) October 01, 2010 Time step 2



(b) October 01, 2010 Time step 3



(a) October 01, 2010 Time step 4



(b) October 01, 2010 Time step 5

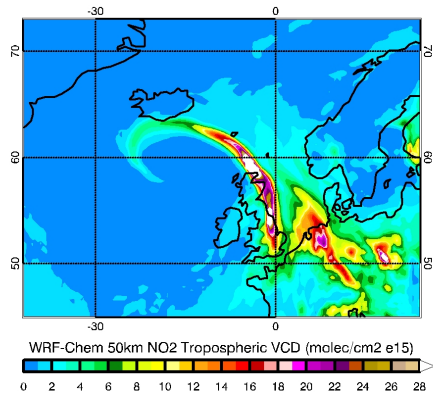
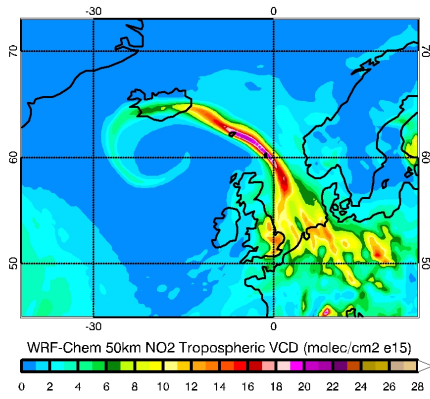
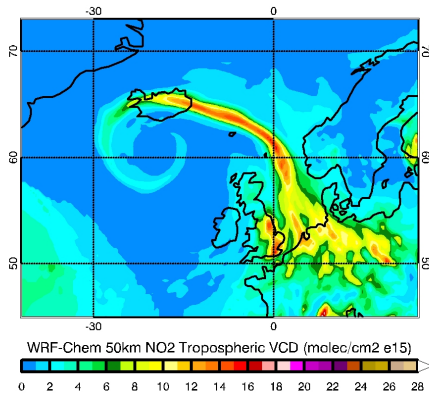


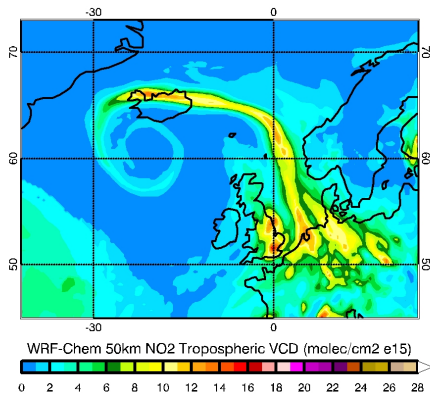
**Fig. A.62.:** October 01, 2010 Time step 6



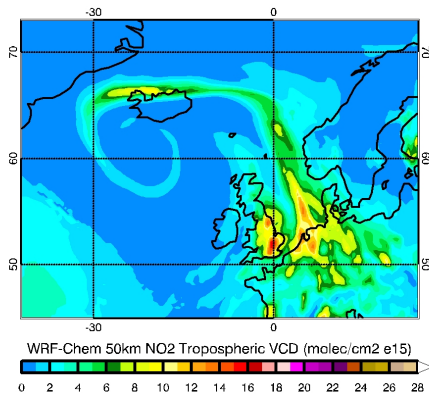
**(a)**October 02, 2010 Time step 0



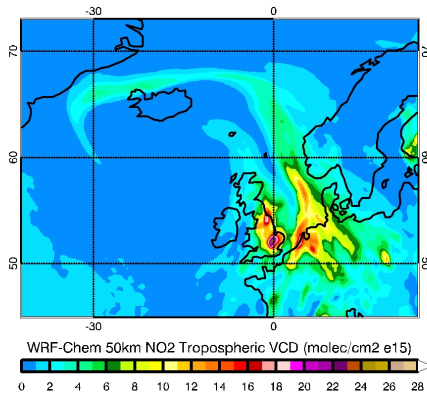
**(b)**October 02, 2010 Time step 1



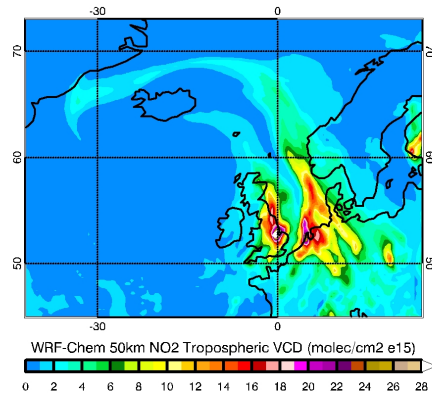
**(a)**October 02, 2010 Time step 2



**(b)**October 02, 2010 Time step 3



(a) October 02, 2010 Time step 4



(b) October 02, 2010 Time step 5

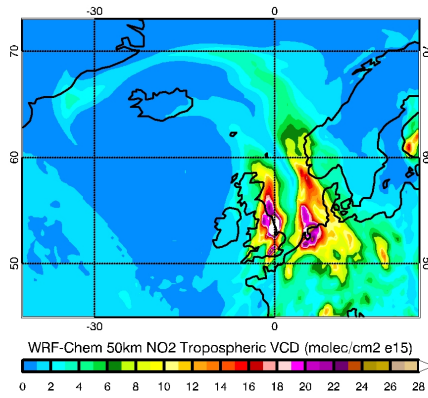
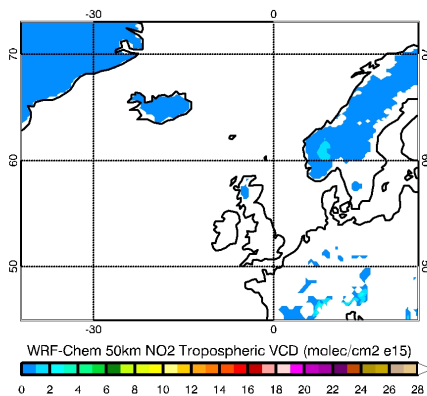
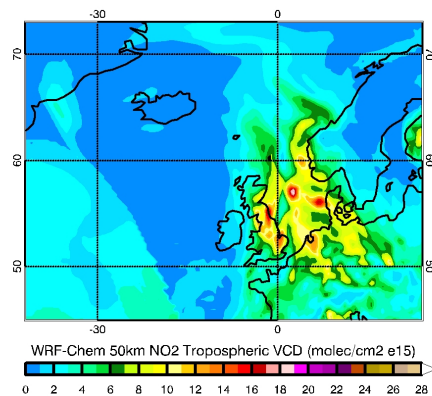


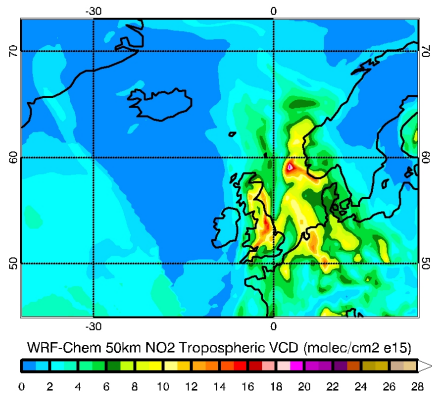
Fig. A.66.: October 02, 2010 Time step 6



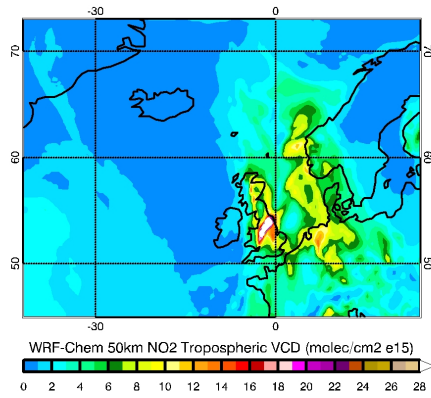
(a) October 03, 2010 Time step 0



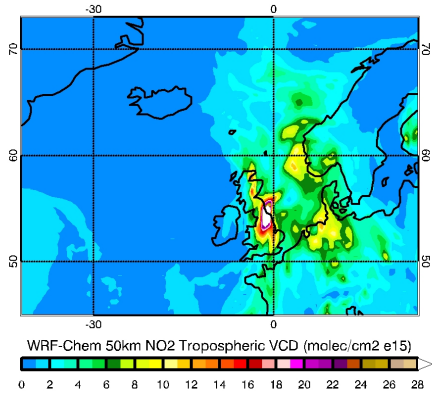
(b) October 03, 2010 Time step 1



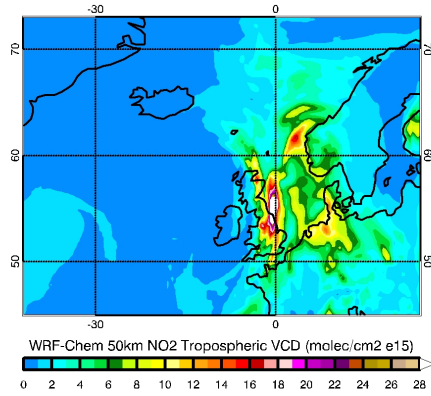
(a) October 03, 2010 Time step 2



(b) October 03, 2010 Time step 3



(a) October 03, 2010 Time step 4



(b) October 03, 2010 Time step 5

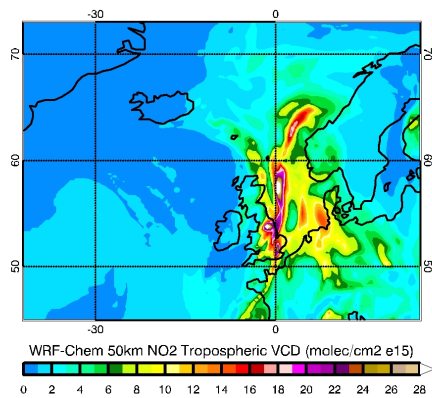
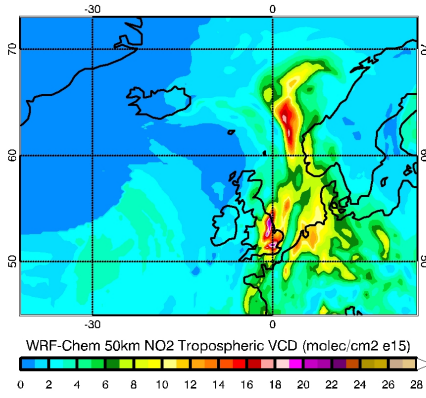
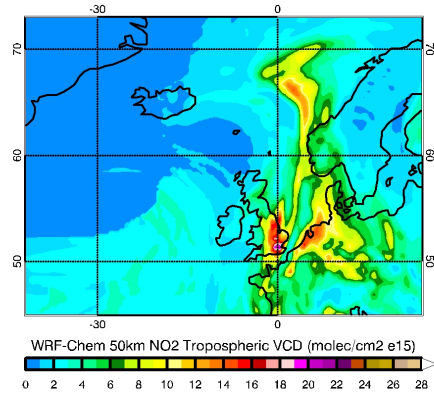


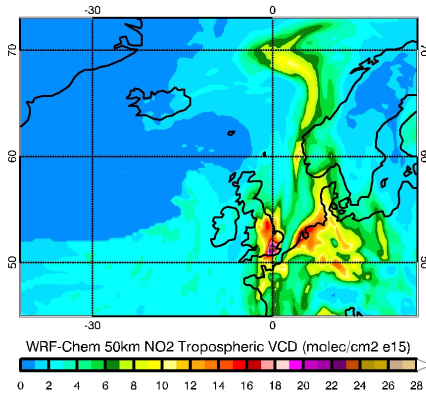
Fig. A.70.: October 03, 2010 Time step 6



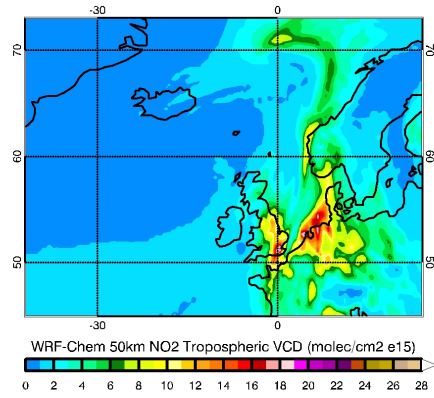
(a) October 04, 2010 Time step 0



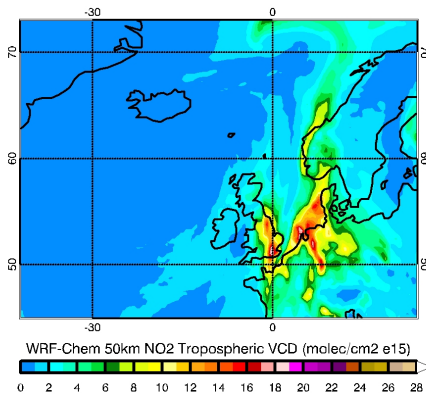
(b) October 04, 2010 Time step 1



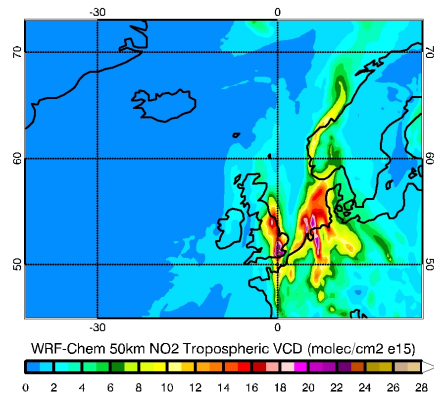
(a) October 04, 2010 Time step 2



(b) October 04, 2010 Time step 3



(a) October 04, 2010 Time step 4



(b) October 04, 2010 Time step 5

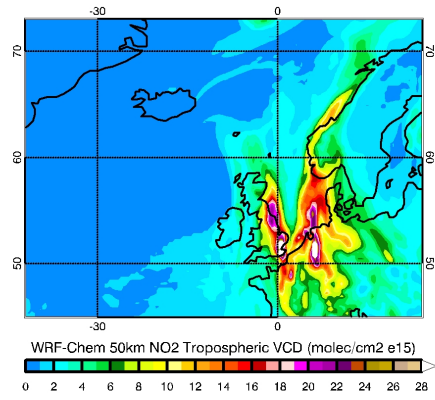


**Fig. A.74.:** October 04, 2010 Time step 6